# Final Report

# Isotopic and geochemical approach to study vulnerable confined and unconfined drinking water aquifer in Varanasi and surrounding areas, India



**NATIONAL INSTITUTE OF HYDROLOGY**
**JAL VIGYAN BHAWAN**
**ROORKEE-247 667**


**2024-25**

## DIRECTOR

**Dr. Manmohan Kumar Goel**

## DIVISIONAL HEAD

**Dr. Y. R. S. Rao**

## PROJECT TEAM

**Dr. Rajesh Singh, Sc. 'E', EHD, NIH Roorkee**
**Dr. S. P. Rai, Associate Professor, BHU, Varanasi**
**Dr. Noble Jacob Sc. G, Hydrology Section, BARC Mumbai**
**Dr. Laszlo Palcsu, ICER, Hungarian Academy of Sciences, Hungary**

# Preface

Water of adequate quality is crucial for supporting socio-economic activities on Earth. However, the increasing levels of pollutants, driven by population growth and economic expansion, are causing significant degradation of water resources. These resources, essential for both direct and indirect human use, are susceptible to contamination from geogenic and anthropogenic sources. Key human activities contributing to water pollution include the release of untreated industrial and municipal wastewater, leachates from solid waste disposal sites, agricultural runoff, fossil fuel combustion, and the vehicular emissions. The excessive extraction of groundwater in the Gangetic Alluvial Plain (GAP) over the past two decades for irrigation, domestic, and industrial purposes has resulted in the overexploitation of these alluvial aquifers. The study area is confined to the Varanasi district and adjoining areas, with a primary focus on assessing water quality. The region is facing water borne diseases due to both surface and groundwater contaminants.

The report has been prepared by Dr. Rajesh Singh (Sc. E, NIH), Dr. Shive Prakash Rai (Associate Professor, BHU, Varanasi), Dr. Noble Jacob (Sc. G, BARC Mumbai), and Dr. Laszlo Palcsu (ICER, Hungarian Academy of Sciences, Hungary).

**(M.K. Goel)**
**Director, NIH**

# Contents

# List of Figures

# List of Tables

# 1. Introduction

More than 3 billion people worldwide depend on water that crosses national borders, but still two billion people rely on faecal contaminated water sources for drinking (WHO, 2023). The UN's (SDGs-6) aim at access to clean drinking water, sanitary conditions, and good hygiene as a fundamental right of every individual, to be universal by the year 2030. As per NITI Aayog report 2018, 21 major cities, including Delhi, Bangalore, and Hyderabad, are expected to reach zero groundwater levels, affecting access for 100 million people. Indian subcontinent has become a water-stressed region with a sharp drop in per capita water availability from a surplus level of 5410 $m^3$ in 1951 to 1614 $m^3$ in 2011 for its population of 1.2 billion (Jain, 2011; UNICEF et al., 2013). In general, the increasing water demands for agriculture, economic activities, power generation, and drinking water has led to inter basin conflicts within the country and also to trans boundary water disputes. Agriculture is the backbone of the country's socioeconomic developments in term of its contribution to the gross domestic product. The water requirement for a projected food production of 250 million metric tons by 2050 and the rising demands for recent economic development underscore the need for sustainable management of groundwater. The groundwater chemistry is a result of numerous factors such as silicate weathering, carbonate dissolution, ion and reverse-ion exchange reactions, redox condition, evaporation, residence time, contamination due to anthropogenic activities (Ansari et al., 2022). A thorough understanding of the hydrological and hydrochemical processes occurring in the multi-tier alluvial aquifer systems is a pre-requisite for the sustainable development and management of water resources in the Middle Ganga Plain. However, very limited work has been done in understanding the hydrogeochemical evolution, spatial and vertical variation of hydrochemical species within an aquifer system of the targeted study which is one of the major intensive agricultural and important urban centers of the Middle Ganga Plain.

Groundwater contamination has also emerged as a serious issue that has posed serious threat to the people living in the Ganga River Basin. Groundwater, which is extensively used for drinking, cooking and/or irrigation, is contaminated with arsenic in many parts of the Ganga Basin and is having severe detrimental effects on human health. Presently, the main problem of depletion of groundwater in Ganga Basin is due to the unsustainable abstraction of groundwater (Rodell et al.,

2009; Tiwari et al., 2009). As the groundwater level is declining, people are drilling to deeper aquifers, to meet the groundwater demand. In the arsenic affected areas, deeper aquifer has been tapped for the extraction of safe groundwater to meet the drinking and other demands. The groundwater extracted from deeper horizons is becoming the most important fresh water resource in Ganga River Basin. However, little is known about the deeper aquifers which are in semi-confined and to confined condition. Understanding the properties of available water resources is a key factor for sustainable water management. These properties include recharge conditions of the infiltration area, safe yield of groundwater, transit times, direction and velocity of an accidental pollution, hydraulic connection between aquifers, water – rock interactions affecting the water quality etc. These processes cannot be understood without an integrated approach of isotope and water chemistry. Therefore, the aim of the present project is to study the hydrogeological properties of aquifer in a part of Middle Ganga Plain using isotope and hydrogeochemical techniques that cannot be otherwise studied by traditional hydrological methods. This investigation will help for better management of the groundwater resources of the study area and it will be a model study for the country too.

## 1.1 Objectives

- Identification of groundwater recharge sources and zones of the aquifer system.
- Estimation of residence time of groundwater.
- Understanding the surface water- groundwater interactions and interconnection of aquifers.
- Understanding the processes of rock water interactions that affect the groundwater quality and assessment of impact of anthropogenic activities on groundwater.

# 2. Study Area

Varanasi city lies along the left bank of the meandering Ganges flowing in the south west north east direction. The city is an important urban center and agrarian dominated region of the Ganga Plain. The district Varanasi fall in the Survey of India toposheet numbers 63K and 63O encompassing an area of 1535 sq.km. The district is divided into 03 administrative tehsils and 08 blocks extending in between latitudes 25° 10′ 30″ to 25° 35′ 15″N and longitude 82° 40′ 50″ to 83° 12′ 18″E with an average elevation of 78m amsl and monotonous flat topography. The district is surrounded by Chandauli in the east, in the north east by Ghazipur, Jaunpur in north and northwest, while south and southwest is surrounded by the districts Mirzapur and Sant Ravidas Nagar respectively. The other closer cities are Azamgarh, Ballia, and Mau which are all part of middle Ganga plain hosting a huge population. Varanasi fall in the humid subtropical climate class (Kottek et al., 2006). The subtropical climate type (Cwa or Cwb) is characterized by hot summers and dry winters with a constant rainfall. The district encounters three different seasons, summer (March-May), monsoon (June-September) and winters (October-February). The temperature drops below 10°C during the winters and rises above 45°C during summers with a relative humidity of 33%, which increases to 70-90% during monsoonal period with an average annual rainfall of 1000 mm (Indian Meteorological Department, 2021).

## 2.1 Geohydrological settings of the study Area

The Indo-Gangetic peripheral foreland basin formed as a consequence of collision between Indian and Asian plate. The flexing of the lithospheric plate in front of the orogen resulted in the formation of underfilled basin which derived its sediments eroded from both Himalayas and the Peninsular India (Figure 2.1).

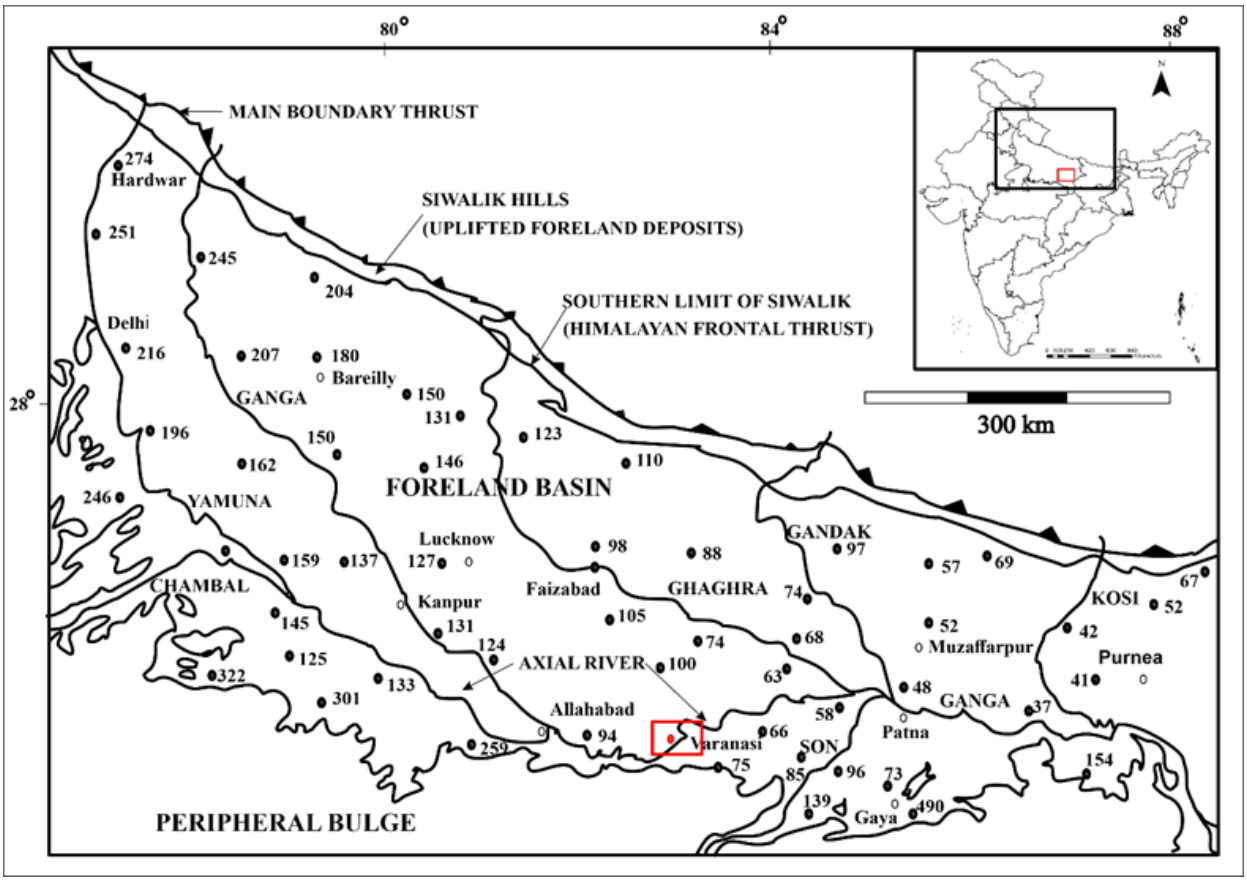


**Figure 2.1**: Inset map showing the Ganga River Basin (GRB), location of the Ganga Plain, Varanasi and adjoining places, major rivers and spot heights (Singh, 1996).

Geologically, Varanasi and surrounding alluvial areas are concealed by older alluvium of middle to upper Pleistocene age and younger quaternary alluvium deposits of upper Pleistocene to Recent age, where older alluvium covers the major part of the district (Figure 2.2). The basement rock being Kaimur sandstone is not exposed but encountered at various depth during borehole drilling (Shukla et al., 2012; Mukherjee et al.,2012; CGWB, 2017). The alluvial geomorphological setting of Varanasi is function of river Ganges and associated Himalayan tectonism, changing climatic conditions, and sea level changes. However, to the south of Varanasi which marks the southern limit of the Ganga alluvial plain is encountered by Vindhyan sedimentary rocks (Singh,1996).

**Table 2.1**: Geological setting of Varanasi and surrounding alluvial dominated regions

| Age | Formation | Lithology |
|---|---|---|
| Upper Pleistocene to Recent | Newer Alluvium | Clay, Sand and Kankar |
| Middle to Upper Pleistocene | Older Alluvium | Fairly consolidated clay with kankar, sand, fine to medium with some gravel |
| Unconformity | | |
| Upper Vindhyan | Kaimur Sandstone | Sandstones, grey to white, buff, arkosic with capping of laterites and Bauxite |

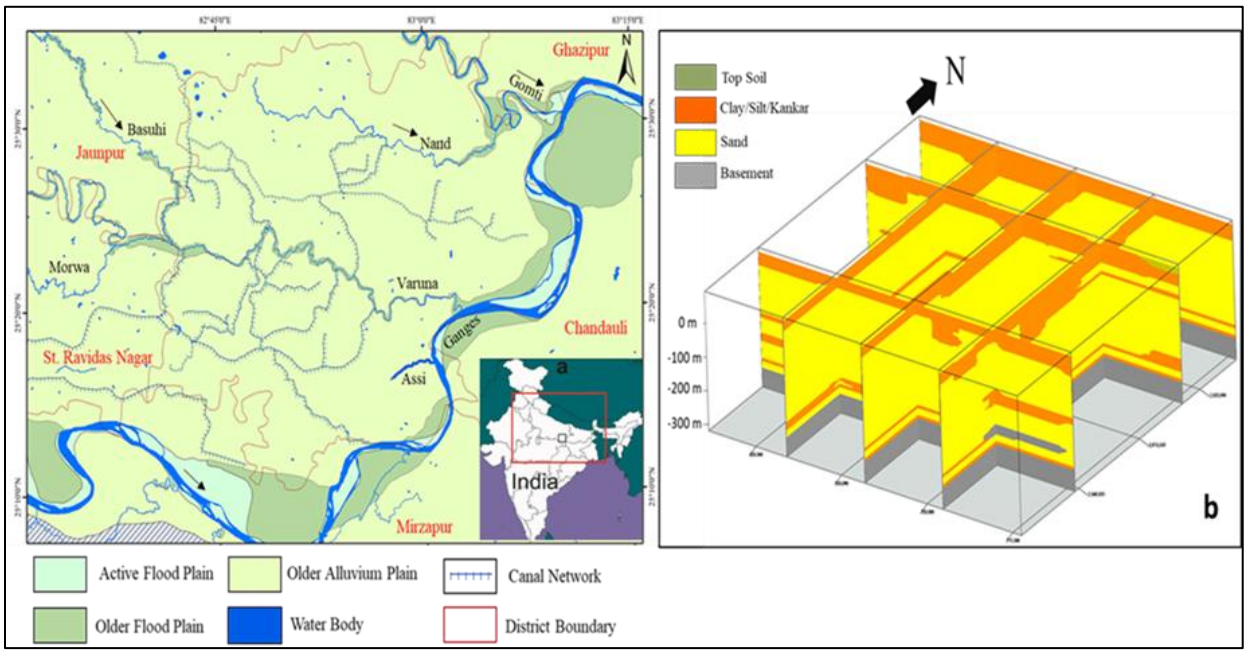


**Figure 2.2**: (a) Inset map showing Ganga Basin and black box corresponds to Varanasi and adjoining areas along with the Geomorphological settings, (b) fence diagram showing abundant clay capping in the entire study area in the upper horizon (surface to 10-15-meter depth).

The principal aquifer systems of the Middle Ganga Plain (MGP) based on lithological and electrical logs has classified into four major types: Aquifer I which varies from soil depth to 150m bgl, Aquifer II 160-240m bgl, Aquifer III 260-370m bgl, and Aquifer IV 370-480m bgl (CGWB, 2020). The mean transmissivity of alluvial aquifer in the Indo-Gangetic Plain reported as

3000$m^2$/day, while hydraulic conductivity varies from 5-100m/day. The specific yield reported for top 200m alluvial aquifer varies from 0.1 to 0.15 (CGWB, 2010; Bonsor et al., 2017). The soil profile sections and geophysical survey confirms the abundance of clay, silt, and kankar nodules up to few meter depths, while iron nodules at some places. The clay abundance has been observed to thicken in the northern part of the study area Fig. 2.2 (CGWB, 2017; GSI, 2021).

# 3. Methodological Framework

The following flowchart (Figure 3.1) was adopted for a comprehensive study of groundwater quality in and around Varanasi. The flowchart represents how results of major, trace metals and environmental isotopes were used to decipher the recharge sources and zones along with identification of the contaminants zones which are very vital for development of management strategies.

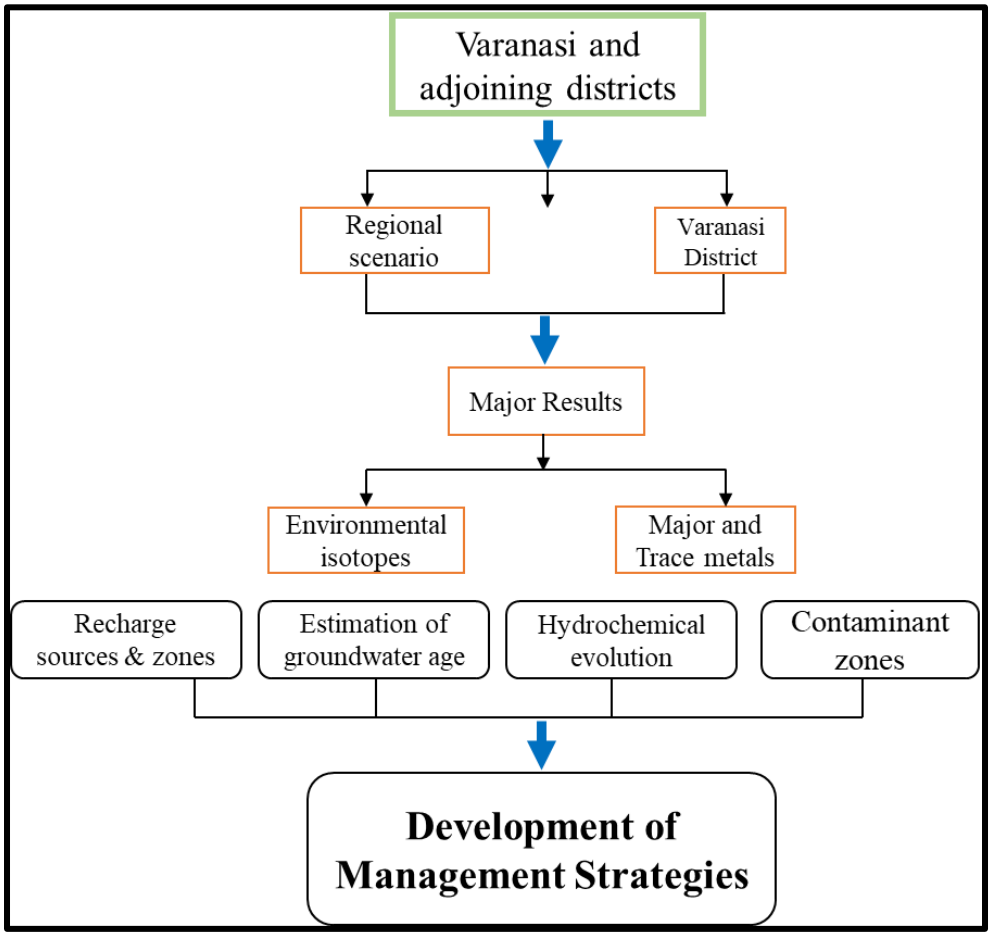


**Figure 3.1**: Methodological framework adopted for this study

## 3.1 Sampling Strategy for major and trace metals

In order to address the groundwater health in the major part of the Middle Ganga Basin (MGP), a grid based, and borehole depth (vertical) groundwater sampling was done for the post-monsoon

season of 2021-22 from Varanasi district. All the water sample collection was done following the standard norms of APHA (2005). The parameters such as geographic coordinate, elevation, temperature, borehole depth, pH, ORP and EC were measured at the sampling sites. Prior to water sample collection wells were purged for a considerable time and groundwater samples from the same well was stored in 120 ml high-density polyethylene (HDPE) bottles for the detailed major ion analysis. A separate set of samples for the trace metals from the same location were treated with ultra-pure $HNO_3$ to bring down the pH<2 in order to minimize the bacterial activities and precipitation of the metal cations and stored in 60ml HDPE. Another set of samples from the same locations were collected in the 15ml HDPE till the brim to avoid any fractionation for stable isotopic analysis ($^{18}O$ and $^{2}H$). Based on the field investigations of borehole depth and in situ parameters selected samples were collected in 500ml HDPE bottles for the tritium ($^{3}H$) analysis. Alkalinity, $HCO_3$- and $CO_3^{2-}$ titrimetrically measured within a day after each grid wise groundwater sampling was done at Hydrogeology Lab, Banaras Hindu University, while major ions were measured within a month after entire groundwater sampling by Metrohm Ion Chromatography (930 Compact IC Flex) at the National Institute of Hydrology, Roorkee, India. Further, the trend of groundwater level (post monsoon 2000 & post – monsoon 2020) was evaluated in the Arc-GIS platform using the IDW interpolation technique. All the groundwater samples after analysis were subject to descriptive statistics and were compared to the given standards BIS (2012) and WHO (2017).

### 3.2 Sampling Strategy for environmental isotopes

Stable isotopes ($^{18}O$ and $^{2}H$) samples were measured at nuclear isotope lab at the National Institute of Hydrology, Roorkee, India. The precision of the isotopic measurements was determined to be **±0.1‰** for **$\delta^{18}O$** and **±1.0‰** for **$\delta^{2}H$**, referenced against the **Vienna Standard Mean Ocean Water (V-SMOW)** on the δ scale. The isotopic ratio (δ) is calculated using the equation:

$$\boldsymbol{\delta = \left(\frac{R_{sample}}{R_{std}} - 1\right) \times 1000}\ ‰\ \textbf{V-SMOW}$$

where, δ is the isotopic ratio, $R_{sample}$ is the ratio of heavier to lighter ($^{18}O/^{16}O$, $^{2}H/^{1}H$) for that given sample, and $R_{std}$ is for the standard (V-SMOW in this case).

For any isotopic studies reference lines are very important to understand the recharge sources and origin of original moisture sources, following reference lines are used for this study.

The regression equation for Global Meteoric Water Line (GMWL); Craig, 1961

**GMWL; $\delta^2H = 8\times\delta^{18}O+10$ (Craig, 1961)**

The regression equation for Indian Meteoric Water Line (IMWL); Kumar et al., (2010)

$$\boldsymbol{\delta^2H = (7.93 \pm 0.06) \times \delta^{18}O + (9.94 \pm 0.51)}$$

Dansgaard (1964), used the relation d-excess= $\delta^2H-8\times\delta^{18}O$; as an index of non-equilibrium conditions which traces the source of the moisture (Kumar et al., 2010; Rai et al., 2023).

**d-excess= $\delta^2H-8\times\delta^{18}O$**

The various spatial variability map was subject to interpolation technique based on minimum square root mean error, and inverse distance weighted (IDW) was best suited for the present study. Various statistical analysis was performed at $p<0.05$ in the IBM SPSS version 26. All the regression lines are made in the Microsoft excel, while bivariate plots are made in the Grapher software. The mineral saturation indices are calculated in the Geochemist work bench community edition version 17.

# 4. Results and Discussions

## 4.1 Water Level Conditions

The annual average rainfall in and around Varanasi for the year 2000 was 902 mm while for 2020 was 805mm (IMD). The depth to water level (bgl) in and around Varanasi for the post monsoon 2020 varied from 0.74 to 12.31 m bgl while the post monsoon 2020 it varied from 0.49 to 21.1 m bgl (Figure 4.1 a & b). The deeper water level is observed in the central and southwest of Varanasi which are extensive agricultural regions while as shallow water level is observed at a few places adjacent to Ganga Bank, which might be due to GW and SW interaction. The general groundwater flow direction follows the surface topography which is from the west to the east. The water level data (post-monsoon 2020) is indication of the shallowest level (0.49 bgl) is around a sparse population and the deepest water level (21.1m bgl) is from Maldahiya (urban Varanasi) which is the most densely populated block (Census, 2011) of the study area indicative of overexploitation of the shallow aquifer in the study area.

A regional depth to water level comparison for post-monsoon 2000 and post-monsoon 2020 shows Urban and semi-urban Varanasi areas have undergone water level decline in last 20 years, even though the rainfall during these years has not varied much. This is result of growing population and unchecked abstraction of shallow groundwater to feed their needs. An interesting highlight of this comparison is in the northwest region of Varanasi water level has not changed much while the north east region along the bank of river Ganga around Ghazipur district water level map shows an increasing trend which might be due to RW-GW interaction (Figure 4.1 a & b). It is also borne that Varanasi being the urban center with higher population density 2395 persons per square km (Census, 2011) has deeper water level than the adjoining districts is indicative of overexploitation of this natural resource.

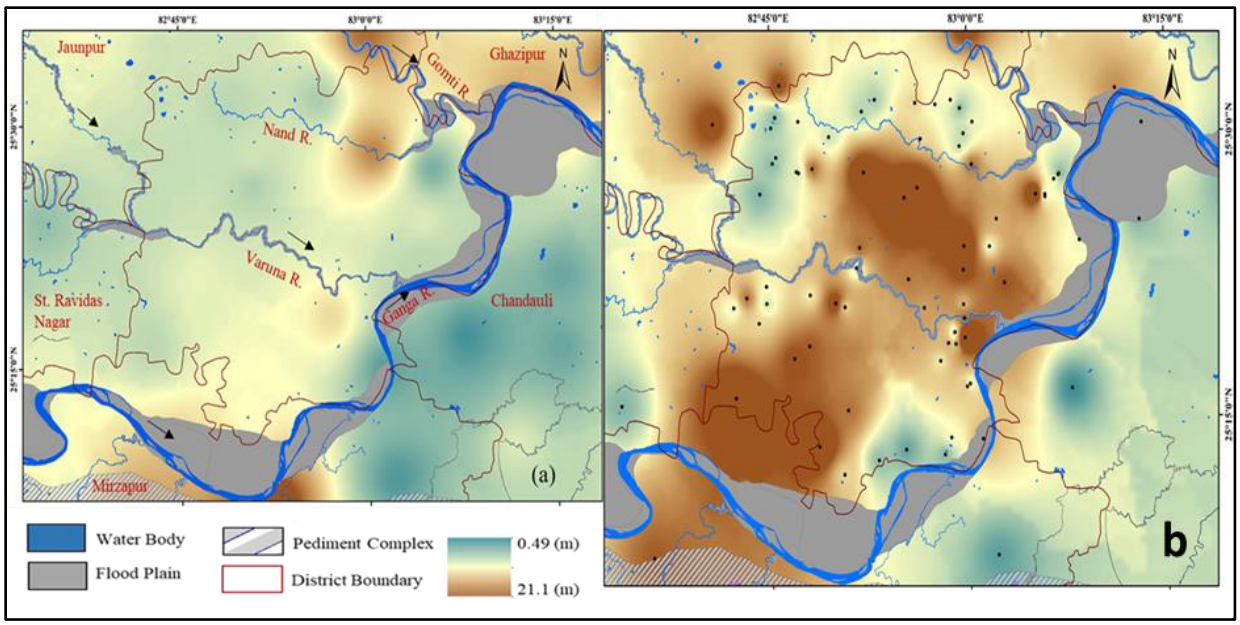


**Figure 4.1**: Regional depth to the water level of Varanasi and adjoining areas (a) post-monsoon 2000 & (b) 2020 along with the geomorphological setting

## 4.2 Groundwater contaminants on a regional scale

The groundwater evolution and its scenario on a regional scale depicts the presence of contaminants $F^-$ and $NO_3^-$ at shallow depths (<50 mbgl). The pH ranged from 7.0 to 9.1, and mean of 8.0, indicative of alkaline groundwater. 5.8 % of the samples exceeded the pH acceptable value set by WHO (2011) and BIS (2012). For Nitrate, it has been observed that out of 7.6% of exceeding samples, 52% of the groundwater samples lie in the agricultural domain while 48% of the samples are located around the built-up area (Figure 4.2). The spatial distribution of nitrate shows two pockets of higher concentration one in the northern part while the other is in the southeastern part. The biogeochemical processes control the nitrate concentrations in the groundwater which may show spatiotemporal variations (Rivett et al., 2008). The use of large amounts of fertilizer in intensive agricultural practices has been reported as the main contributor to nitrate pollution in the groundwater (Nas & Berktay 2006). Field investigation conforms that nitrate-dominated areas are waterlogged, and the low water table facilitates the transport of fertilizers applied to crops which is nitrate source for the 52% of contaminated groundwater samples. The remaining 48% of the exceeding nitrate levels in the groundwater samples around residential area is due to the leaky septic, drain systems, urban forest, and grasslands (Zhou et al., 2015). Moreover, increasing

number of nitrogen-laden wastewater from industries has also triggered the enrichment of nitrate in the groundwater system.

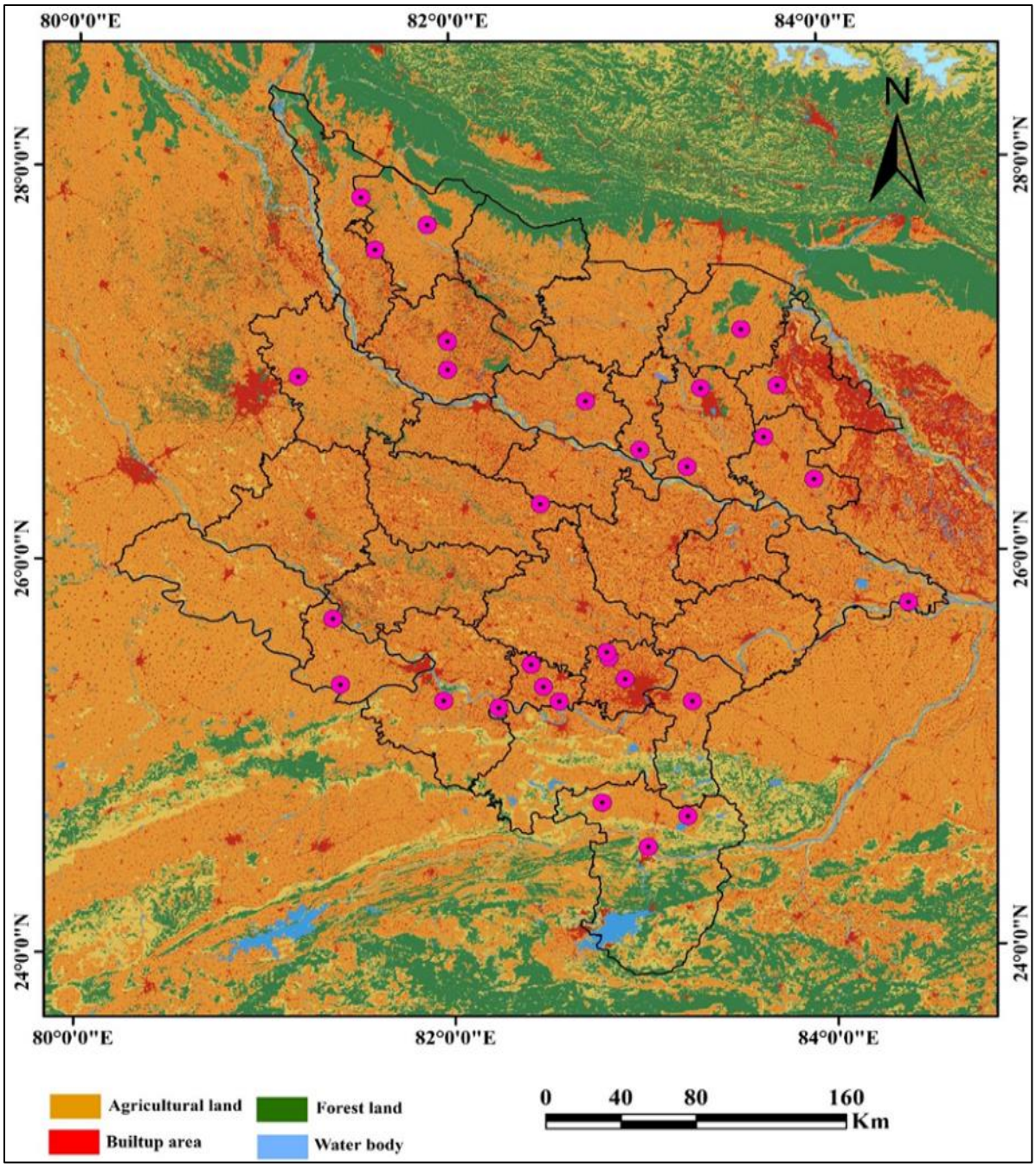


**Figure 4.2**: LULC for Nitrate >45 (mg/L), shows 52% of the samples falling in the agriculture field while 48% of the samples fall in the residential area, clearly depicting the anthropogenic control on nitrate contamination of the study area.

The spatial distribution map (Figure 4.3) shows the exceeding values of fluoride mainly lie in Yamuna and Sai alluvial zone except for three samples. Most of the tributaries of Yamuna flow over the peninsular craton, consisting of crystalline rocks having granitic composition. Fluoride-bearing minerals such as fluorapatite, fluorite (fluorspar), mica, and amphibole group minerals contribute to high fluoride concentration in the groundwater in the study area (Raju et al., 2009; Samal et al., 2020; Pant et al., 2021; Nizam et al., 2022). All this coherence and previous findings confirm the geogenic release of the $F^-$ into the groundwater of Middle Ganga Basin (MGB).

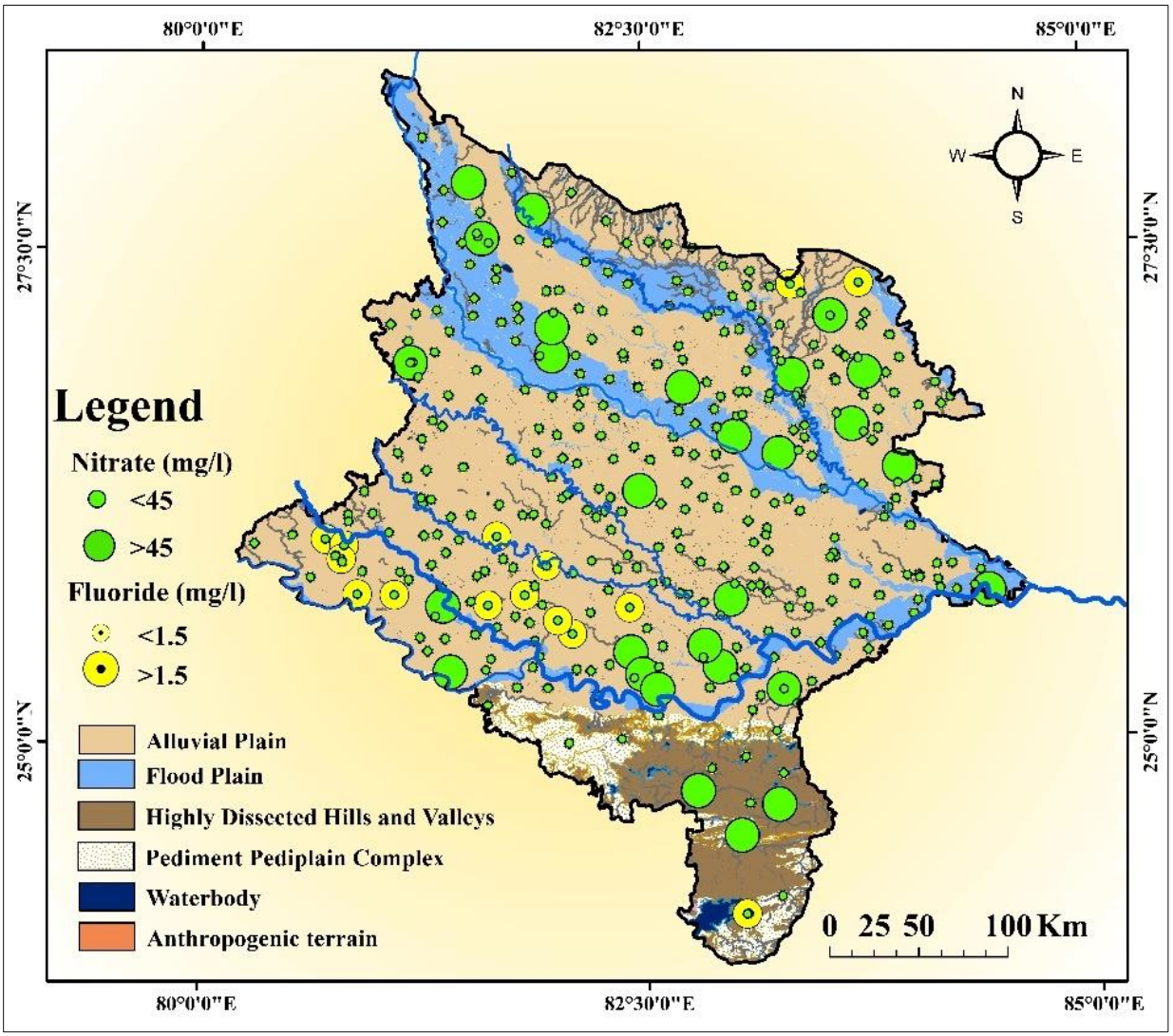


**Figure 4.3**: Fluoride exceeding samples are mostly related to geogenic minerals such fluorite, mica and amphiboles

### 4.3 Groundwater Scenario in Varanasi District

Water quality assessment is an integral part, which decides its utility for drinking, agricultural and industrial purposes World Health Organization (WHO, 2011). The statistical summary of various physicochemical parameters of groundwater samples are presented in (Table 4.1). The borehole depth of various wells tapping at different levels of the alluvial aquifer varied from 2.2m (bgl) to 213.4 m (bgl), respectively with a mean borehole depth of 63.2 (±43) m (bgl). The pH ranges from 7.1 to 8.3 with a mean value of 7.5 (±0.7), showing groundwater is circumneutral to alkaline in nature. The EC ranges from 440 µS/cm to 2630 µS/cm with a mean of 902 (±362.2) µS/cm, of which 4.8 % of the samples exceeding the permissible limit BIS (2015). The major cationic and anionic abundance follows an order of $Na^+ > Ca^{2+} > Mg^{2+} > K^+ > Li^+$ and $HCO_3^- > SO_4^{2-} > Cl^- > NO_3^- > F^-$ respectively while overall mean ionic contribution suggests an order of $HCO_3^- > Na^+ > SO_4^{2-} > Ca^{2+} > Mg^{2+} > Cl^- > NO_3^- > F^-$. The $HCO_3^-$ varies in between 205 mg/L to 1138 mg/L with a mean value of 415 (±119.7) mg/L and 6.8 % of the samples exceeding the permissible limit BIS (2015). The release of $HCO_3^-$ is commonly attributed to alumino silicate minerals and carbonate weathering, while carbonate precipitation can subsequently lower its concentration in the groundwater. The $Cl^-$ ion concentration varies in between 0.9 mg/L to 345 mg/L with the mean value of 36 (±56.3) mg/L. The $SO_4^{2-}$ ion concentration in the groundwater varies from 0.7 mg/L to 1707 mg/L with mean value of 61 (±200.6) mg/L and 2.1% of the samples exceeding the permissible limit. The $NO_3^-$ value in the groundwater varies from 0.01 mg/L to 211.7 mg/L with a mean value of 12.2 (±22.4) mg/L and 4.8 % of the groundwater samples exceeding the permissible limit BIS (2015). High nitrate concentration generally above 10 (mg/L) and its mobilization in groundwater are mainly linked to human inputs through N- fertilizers, sewage return, domestic waste (Akpataku et al., 2020; Pant et al., 2021; Kumar et al., 2021). The $F^-$ in the groundwater samples varies from 0.27 mg/L to 4.2 mg/L with a mean of 0.8 (±0.6) mg/L and 7.5 % of the groundwater samples exceeding the permissible limit BIS (2015). The release of $F^-$ ion in groundwater is generally attributed to the dissolution of silicate bearing minerals such as mica, apatite, fluorspar, amphiboles. On comparing the $Na^+$, $K^+$, and $Mg^{2+}$ concentrations with their permissible limits it is observed that 11.6 %, 1.4 %, and 1.4 % of the groundwater samples exceeded their respective limits as per given standards (BIS 2012, WHO 2017). The release of these ions is attributable to silicate and carbonate weathering, also a lot of cations especially $Na^+$ are released through highly soluble saline and alkaline soils of $Na_2CO_3$, $NaHCO_3$ occurring in the

Ganga Alluvial Plain (Singh et al., 2010; Chatterjee and Singh, 2022). Apart from these ion exchange processes, and precipitation of some ions can increase the relative concentration of other. Overall, the groundwater is fresh but hard to very hard type based on the total hardness.

**Table 4.1**: General Statistics of various physico chemical parameters of groundwater samples

| Parameter | Mean | Min | Max | Std. Dev. | Skewness | WHO (2017) | BIS (2012) | % Exceeding |
|---|---|---|---|---|---|---|---|---|
| BD (m) | 63.2 | 2.2 | 213.4 | 43.0 | 1.1 | | | |
| pH | 7.5 | 7.1 | 8.3 | 0.2 | 0.7 | 6.5-8.5 | 6.5-8.5 | |
| EC (µS/cm) | 902.1 | 440 | 2630.0 | 362.2 | 2.2 | | 1500 | 4.8 |
| TDS (mg/L) | 514.4 | 230.0 | 1395.2 | 209.2 | 1.7 | | 500-2000 | |
| Temp (°C) | 26.4 | 22.4 | 28.4 | 1.0 | -1.0 | | | |
| Alkalinity | 354.7 | 173.3 | 933.3 | 110.6 | 1.4 | | | |
| $CO_3$ (mg/L) | 9.7 | <BDL | 72.0 | 13.5 | 1.6 | | 200-600 | |
| $HCO_3$ (mg/L) | 415.8 | 205.0 | 1138.7 | 119.7 | 1.8 | | 600 | 6.8 |
| F (mg/L) | 0.8 | 0.2 | 4.2 | 0.6 | 3.2 | 1.5 | 1-1.50 | 7.5 |
| Cl (mg/L) | 36.0 | 0.9 | 344.9 | 56.3 | 3.0 | | 250-1000 | |
| $NO_3$ (mg/L) | 12.2 | 0.01 | 211.7 | 22.4 | 5.8 | 50 | 45 | 4.8 |
| $SO_4$ (mg/L) | 61.4 | 0.7 | 1707.7 | 200.6 | 6.5 | 200-400 | 200-400 | 2.1 |
| Li (mg/L) | 0.0 | <BDL | 1.1 | 0.1 | 10.2 | | | |
| Na (mg/L) | 88.1 | 6.4 | 664.6 | 103.2 | 3.2 | 200 | | 11.6 |
| K (mg/L) | 4.0 | 0.9 | 34.2 | 3.2 | 6.3 | 12 | | 1.4 |
| Ca (mg/L) | 55.2 | 12.7 | 133.9 | 18.4 | 1.0 | | 75-200 | |
| Mg (mg/L) | 39.9 | 10.2 | 109.1 | 17.7 | 1.4 | | 30-100 | 1.4 |
| TH (mg/l) | 301.5 | 96.7 | 782.9 | 94.0 | 1.7 | | | |

### 4.3.1 Spatial variability of various physico chemical parameters

The spatial variability map shows most of the study area is characterized by TDS (mg/l) ranging in between 500-1000 (mg/l), which is within the acceptable limits as per the given standards BIS 2012 (Table 4.1). However, TDS within 500 mg/l is observed in a few pockets like central, southwestern regions. The pH is the concertation of the proton $H^+$ in the water system, for the present study it can be observed most of the study area is dominated by an alkaline water (pH>7), however, more alkaline water (pH 7.6 -8) can be observed in the central, north eastern, and south eastern regions. As per the given standards (Table 4.1), all groundwater samples are within the permissible limit of the pH values.

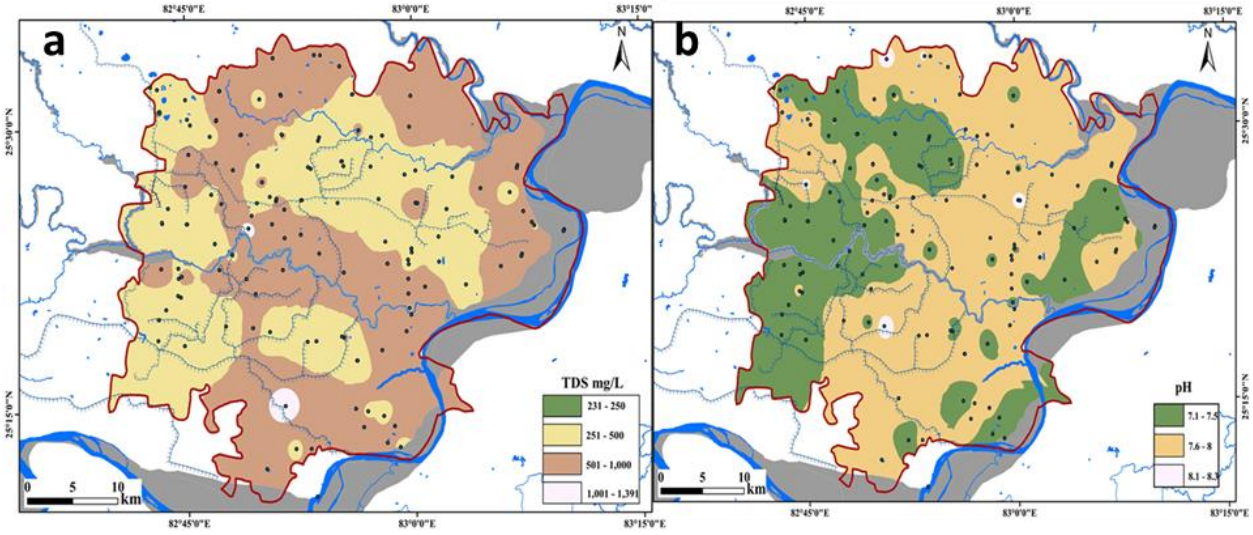


**Figure 4.4**: Spatial variability maps of TDS (mg/l) and pH of the groundwater prepared using IDW interpolation technique

The calcium concentration ($Ca^{2+}$) in the study area shows major range in between 51-75 mg/l in most part of study area (Fig. 5 a), however lower concentration in the northwestern region, northern, northeastern and southwestern regions can be observed. A few, isolated pockets $Ca^{2+}$ can be seen in the central and southern parts of the study area (Figure 4.5a). The Magnesium concentration ($Mg^{2+}$) shows most of the groundwater samples are within the range of 30-50 mg/l (Figure 4.5b), with some patches in the north western in which concentration >50 mg/l can be observed, while concentration <30 mg/l can be seen in small pockets in southern, and north eastern regions (Fig. 4.5 b). It is evident that study area is covered by older alluvium (Figure 2.2b), in

which formation of calcrete is a dominant process due to alternate dry and wet seasons, and their dissolution releases abundant $Ca^{2+}$ and $Mg^{2+}$ into the groundwater (Raju, N.J., 2012).

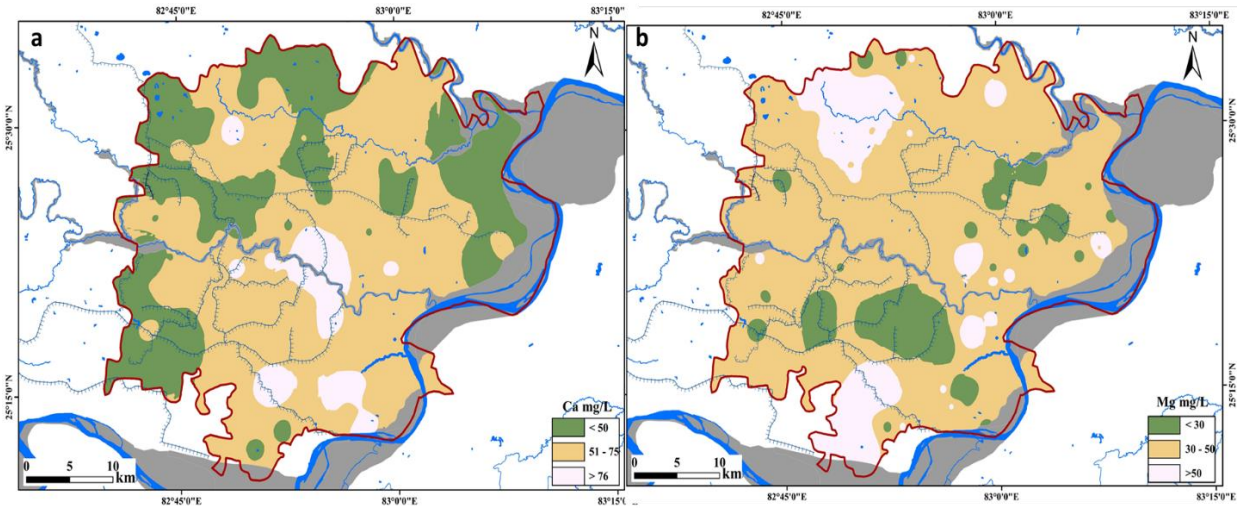


**Figure 4.5**: Spatial variability maps of $Ca^{2+}$ (mg/l) and $Mg^{2+}$ of the groundwater samples in the study area prepared using IDW interpolation technique.

The spatial variability map of sodium ($Na^{+}$) shows most of the groundwater samples are within the limit of the given standard of WHO (2017), which is 200 mg/l (Table 4.1). However, in the north western region of the study area $Na^{+}$ concertation is observed in between 200-400 mg/l Figure 4.6a.

The most of the groundwater samples are within the limit of $K^{+}$ concertation, however, a very small patch of $K^{+}$ concentration is observed above the given standard of 12 mg/l in the northern region (Figure 4.6b). The soil mineralogy reveals abundance of minerals like albite, orthoclase, amphiboles, micas, chlorite, and illite, while saline and alkaline soils of $Na_2CO_3$, $NaHCO_3$ is quite common in the study area especially in the north western region part of the study area (GSI, 2021; Chatterjee and Singh, 2022). The dissolution of these minerals releases abundant $Na^{+}$, $K^{+}$, $Ca^{2+}$, and $Mg^{+}$ as reflected in the groundwater chemistry of the present study.

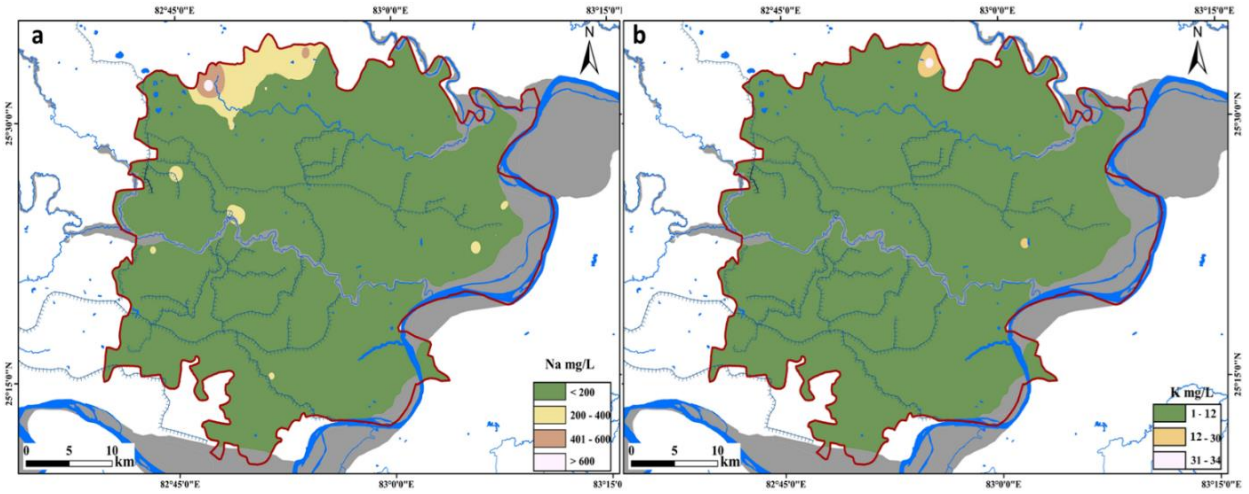


**Figure 4.6**: Spatial variability maps of $Na^+$ (mg/l) and $K^+$ (mg/l) of the groundwater samples in the study area prepared using IDW interpolation technique.

The spatial variability of the major ions shows most of the groundwater samples are within the permissible limit of the chloride ($Cl^-$) concentration (Figure 4.7a), however a relative enriched chloride zones can be seen in the north western and southern part of the study area. The spatial variability of the sulphate ($SO_4^{2-}$) is suggestive of a relative higher concentration in the north western regions, since most of the groundwater samples fall within 400 mg/l, which is considered safe as per the given standards BIS 2012, and WHO 2017 (Table 4.1). The higher concentration of these ions can be attributable to human activities (Akpataku et al., 2020).

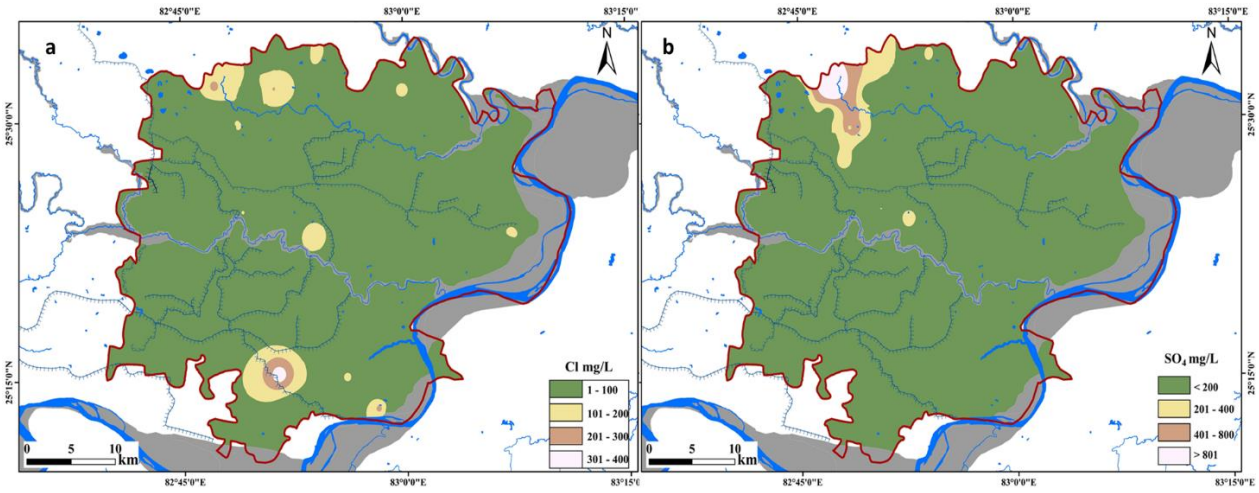


**Figure 4.7**: Spatial variability maps of $Cl^-$ (mg/l) and $SO_4^{2-}$ (mg/l) of the groundwater samples in the study area prepared using IDW interpolation technique.

The primary investigations reflect nitrate affected groundwater samples are from the shallow groundwater tapping the aquifer up to a depth of 100 m(bgl) and all the samples are from Indian Mark II Handpump except one which is from the dug well. No spatial trend (Figure 4.8a) is observed in the nitrate exceeding wells the primary field investigation suggests majority of the groundwater nitrate enriched samples 75% are from the agricultural field while 25% of the nitrate rich samples are from the human settlement area. Thus, the use of chemical fertilizers in an agrarian dominated region and domestics wastes, leaky septic tank are the most probable reasons which contaminate the groundwater locally and are less prominent at a larger scale (Fetter, 1999). The spatial variability of the $F^-$ shows enriched zones in the north western, and north eastern regions (Figure 4.8b), which also happened to be shallow groundwater level zones (Figure 4.1b). These regions also show relatively lower concentration of $Ca^{2+}$ ion and relatively higher pH and $Na^+$ concentration in the groundwater. All these variations reflect $F^-$ enrichment into the groundwater due to silicate minerals releasing $F^-$ and $Na^+$ under alkaline water-logged conditions.

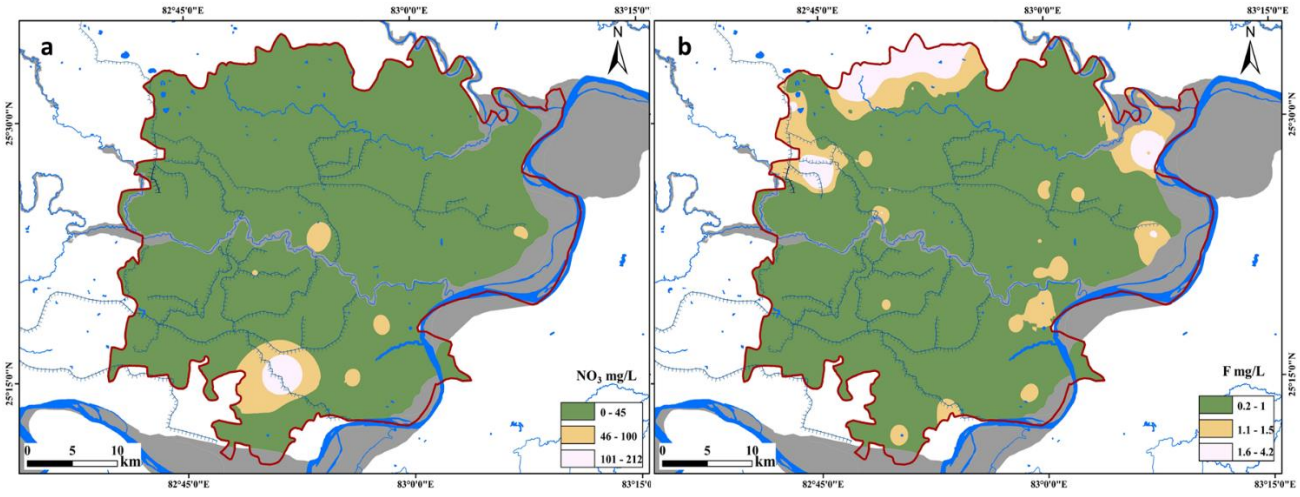


**Figure 4.8**: Spatial variability maps of $NO_3^-$ (mg/l) and $F^-$ (mg/l) of the groundwater samples in the study area prepared using IDW interpolation technique.

### 4.3.2 Groundwater classification based on vertical distribution of various physiochemical parameters

The ionic concentrations of $SO_4^{2-}$, $NO_3^-$, EC, and $Cl^-$ were plotted against borehole depths (Figure 4.9 a-d) to examine the depth-wise distribution of hydrochemical parameters in the alluvial aquifers of Varanasi district. The vertical variation reveals elevated concentrations of EC, $NO_3^-$, $Cl^-$, and $SO_4^{2-}$ up to a borehole depth of 100 m bgl, followed by a noticeable decline in their concentrations beyond 100 m bgl.

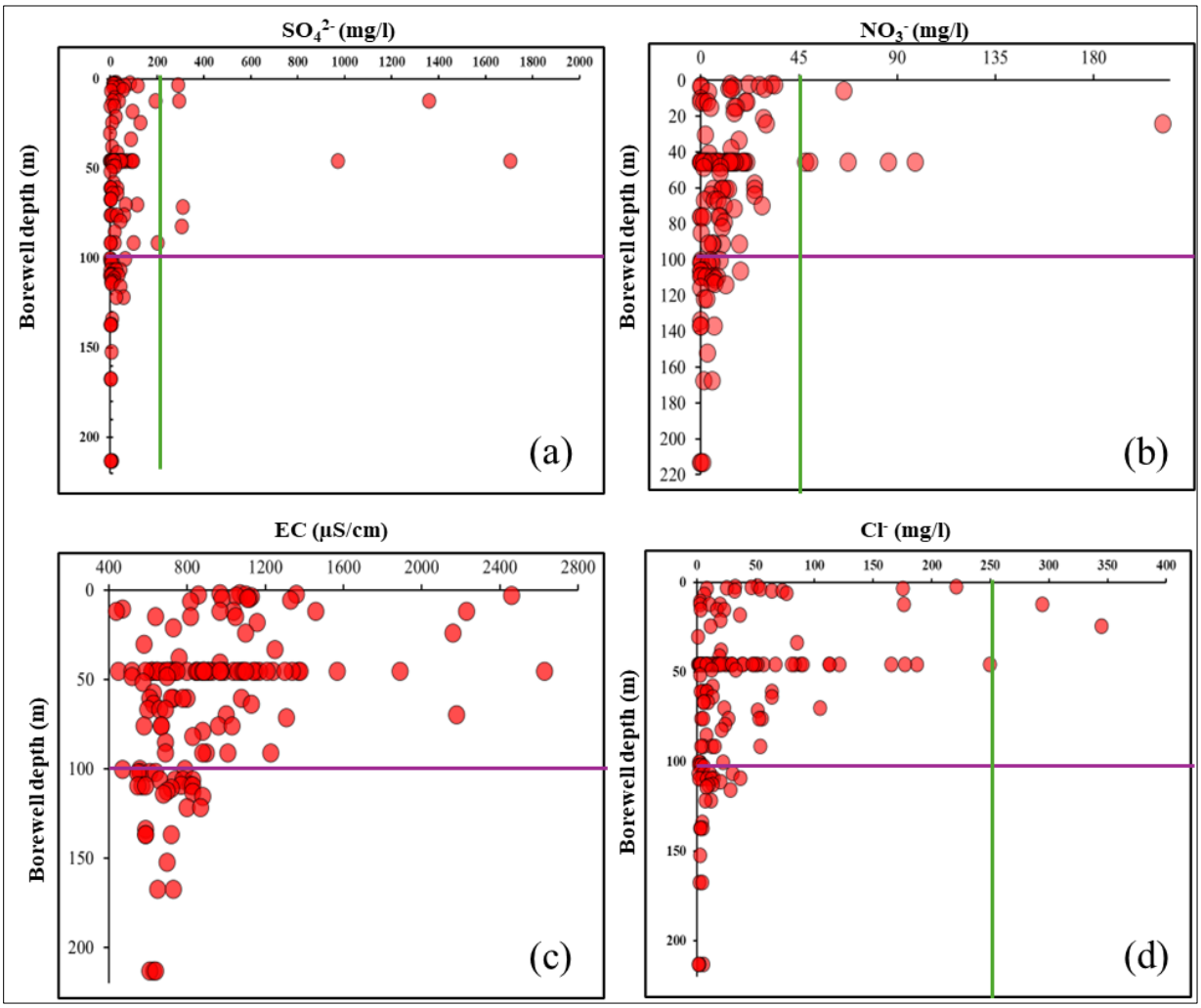


**Figure 4.9**: (a) $SO_4^{2-}$ vs borewell depth, (b) $NO_3^-$ vs borewell depth, (c) Electrical Conductivity (µs/cm) vs borewell depth, and $Cl^-$ vs borewell depth

Based on the chemical and stable isotopic signatures of groundwater, as well as the subsurface framework, the first aquifer extending up to 150 m (CGWB, 2020) has been further categorized into two zones: **Zone 1**, up to a depth of 100 m bgl, referred to as the 'G1 group' of groundwater samples, and **Zone 2**, ranging from 100 to 210 m bgl, referred to as the 'G2 group' of groundwater samples.

The G1 group primarily includes groundwater from open dug wells, Indian Mark-II hand pumps, and small private bore wells with submersible pumps installed at depths up to 100 m (Lapworth et al., 2018; Das et al., 2021). In contrast, the G2 group consists of groundwater samples predominantly from deeper parts of the first aquifer (beyond 100 m) and the second aquifer (160–240 m).

To validate this classification into G1 (depth: <100 m) and G2 (depth: 100–210 m), a depth-wise profiling of hydrochemical species was conducted. Additionally, a comparison of descriptive statistics for groundwater samples from the two groups was performed, along with a Mann-Whitney U-test at a significance level of $p < 0.05$ (Table 4.2).

Both descriptive analysis ($p < 0.05$) and the Mann-Whitney U-test ($p < 0.01$) at a 1% significance level (Z ±2.58) clearly differentiate the two groups of groundwater samples based on various physicochemical parameters (Table 4.2). The results indicate that major concentrations of hydrochemical species such as $NO_3^-$, $Cl^-$, $SO_4^{2-}$, and EC are predominantly found in the G1 group (<100 m), supporting the proposed vertical classification scheme for groundwater samples.

**Table 4.2**: Physicochemical parameters for groups G1 & G2, along with Mann Whitney U-test for G1 & G2 respectively

| | G1 (up to 100m) | | | G2 (>100m-210m) | | | Mann Whitney U test | |
|---|---|---|---|---|---|---|---|---|
| **Parameter** | **Min** | **Max** | **Mean** | **Min** | **Max** | **Mean** | **Z value** | **p-value** |
| BD(m) | 3.0 | 91.4 | 44.1 | 100.6 | 213.4 | 125.9 | | |
| pH | 7.0 | 8.3 | 7.5 | 7.1 | 8.3 | 7.5 | 0.5 | 0.58 |
| EC (µS/cm) | 325.0 | 2630.0 | 957.0 | 470.0 | 880.0 | 683.8 | 4.9 | 0.00 |
| TDS (mg/L) | 142.0 | 1395.2 | 547.9 | 289.0 | 477.0 | 375.9 | | |
| Temp (°C) | 22.4 | 28.4 | 26.3 | 24.5 | 28.3 | 26.9 | | |
| Alkalinity (mg/L) | 173.3 | 933.3 | 376.3 | 213.3 | 373.3 | 284.3 | 4.5 | 0.00 |
| $CO_3^{2-}$ (mg/L) | <BDL | 72.0 | 10.6 | <BDL | 24.0 | 6.8 | | |
| $HCO_3^-$ (mg/L) | 205.0 | 1138.7 | 437.8 | 270.0 | 447.3 | 343.3 | | |
| $F^-$ (mg/L) | 0.2 | 4.2 | 0.9 | 0.2 | 0.8 | 0.5 | | |
| $Cl^-$ (mg/L) | 0.9 | 344.9 | 44.2 | 1.3 | 37.1 | 9.0 | 4.7 | 0.00 |
| $NO_3^-$ (mg/L) | 0.4 | 211.7 | 14.9 | <BDL | 18.4 | 3.5 | 4.5 | 0.00 |
| $SO_4^{2-}$ (mg/L) | 0.7 | 1707.7 | 75.9 | 1.5 | 66.1 | 14.3 | 2.9 | 0.00 |
| $Li^+$ (mg/L) | <BDL | 1.1 | 0.0 | <BDL | 0.0 | 0.0 | | |
| $Na^+$ (mg/L) | 6.4 | 664.6 | 101.6 | 12.4 | 106.2 | 43.7 | 3 | 0.00 |
| $K^+$ (mg/L) | 0.9 | 34.2 | 4.1 | 1.7 | 6.2 | 3.5 | -0.09 | 0.0 |
| $Ca^{2+}$ (mg/L) | 12.7 | 133.9 | 56.7 | 32.6 | 77.6 | 50.6 | 1.9 | 0.05 |
| $Mg^{2+}$ (mg/L) | 10.2 | 109.1 | 42.4 | 11.6 | 46.4 | 31.7 | 3.3 | 0.00 |
| TH (mg/l) | 96.7 | 782.9 | 315.2 | 189.7 | 324.3 | 256.5 | | |

### 4.3.3 Understanding the processes of rock water interactions that affect the groundwater quality

Groundwater chemistry evolves due to reactive interactions between recharging water, soil, and the aquifer matrix, as well as anthropogenic activities or a combination of both (Mukherjee and Fryar, 2008; Singh et al., 2022). In the Ganga Plain aquifers, groundwater mineralization is primarily governed by silicate weathering (both primary and secondary), carbonate dissolution, and cation exchange processes (Singh, 1996).

The Gibbs (1970) plot (Figure 4.10) reveals that rock-dominant processes, such as water-rock interactions, are the main contributors to the major ion content in groundwater samples for both groups. The incremental ratio $Na^+/(Na^+ + K^+ + Ca^{2+})$ further confirms that rock-water interactions control the groundwater chemistry in these groups (Figure 4.10). However, a few groundwater samples from the G1 group exhibit a slight shift towards the evaporation domain, whereas the G2 group samples consistently fall within the rock-water interaction domain.

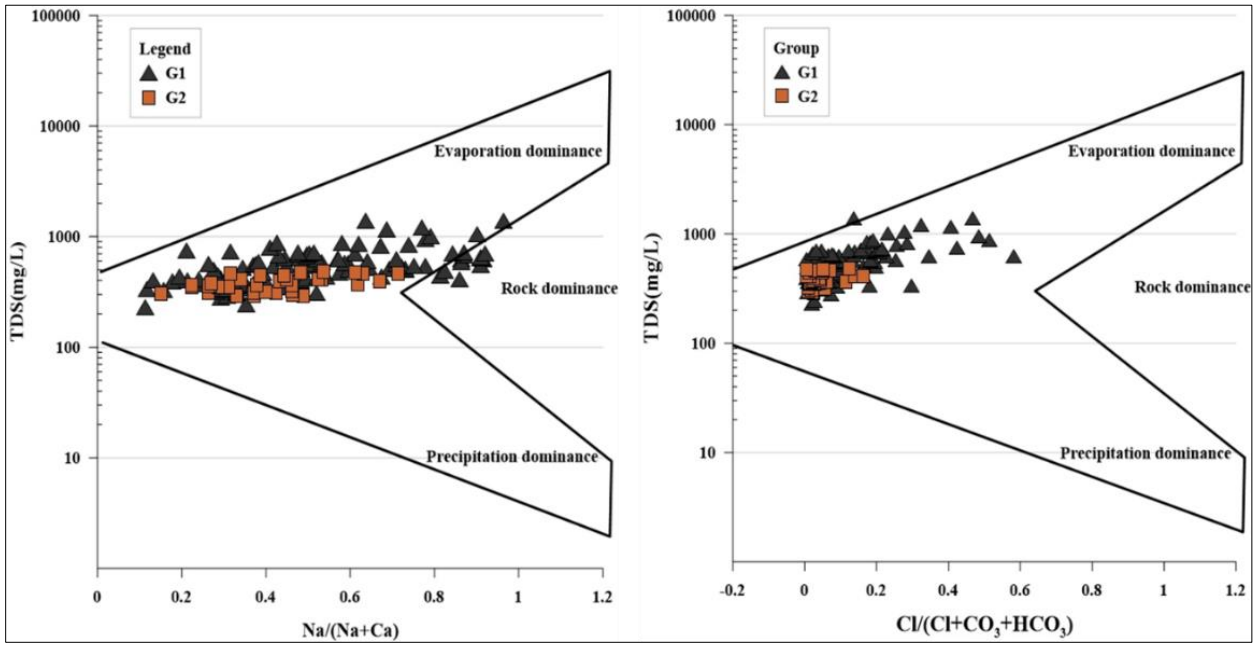


**Figure 4.10**: Gibbs diagram for G1 (up to 100 mbgl) and G2 (>100-210 mbgl) groundwater samples

The calculation of Saturation Indices (SIs) (Fetter, 1988) provides insights into groundwater equilibrium conditions with potential reactive minerals in the soil or aquifer matrix, without requiring direct collection of soil or aquifer mineral data. An SI value of 0 indicates that a mineral is in equilibrium with the groundwater, a negative SI value suggests undersaturation (the mineral may dissolve), and a positive SI value indicates oversaturation (the mineral may precipitate).

For the G1 group, 73% and 27% of groundwater samples are saturated and oversaturated with respect to aragonite, respectively. Regarding calcite, 48% of the samples are in equilibrium, while 52% are oversaturated. All samples (100%) in this group are oversaturated with dolomite, whereas for fluorite, 8% are saturated and 92% are undersaturated (Figure 4.11 a-d).

In the G2 group, 82% and 18% of samples are in saturation and oversaturation states, respectively, for aragonite. For calcite, 74% are saturated and 26% oversaturated. In contrast, all samples (100%) are undersaturated with respect to both dolomite and fluorite (Figure 4.11 a-d).

These variations in mineral saturation indices are critical for identifying underlying hydrogeochemical processes that regulate groundwater chemistry (Chidambaram et al., 2011). The relationship between total cations (TZ+) and the sum of sodium and potassium (Na+ + K+) (Figure 4.12c) reveals distinct hydrogeochemical processes. Samples plotting above the (Na+ + K+) = 0.3TZ+ line exhibit increasing sodium and potassium concentrations with increasing mineralization, indicating silicate weathering and preferential sodium release over alkaline earth metals (Stallard and Edmond, 1987; Senthilkumar and Elango, 2013; Kanagaraj and Elango, 2019). Conversely, samples falling below the line suggest dominance of calcium and magnesium, likely controlled by carbonate dissolution or the presence of calcium- and magnesium-bearing minerals in the subsurface (Shukla and Raju, 2009; Patel et al., 2024).

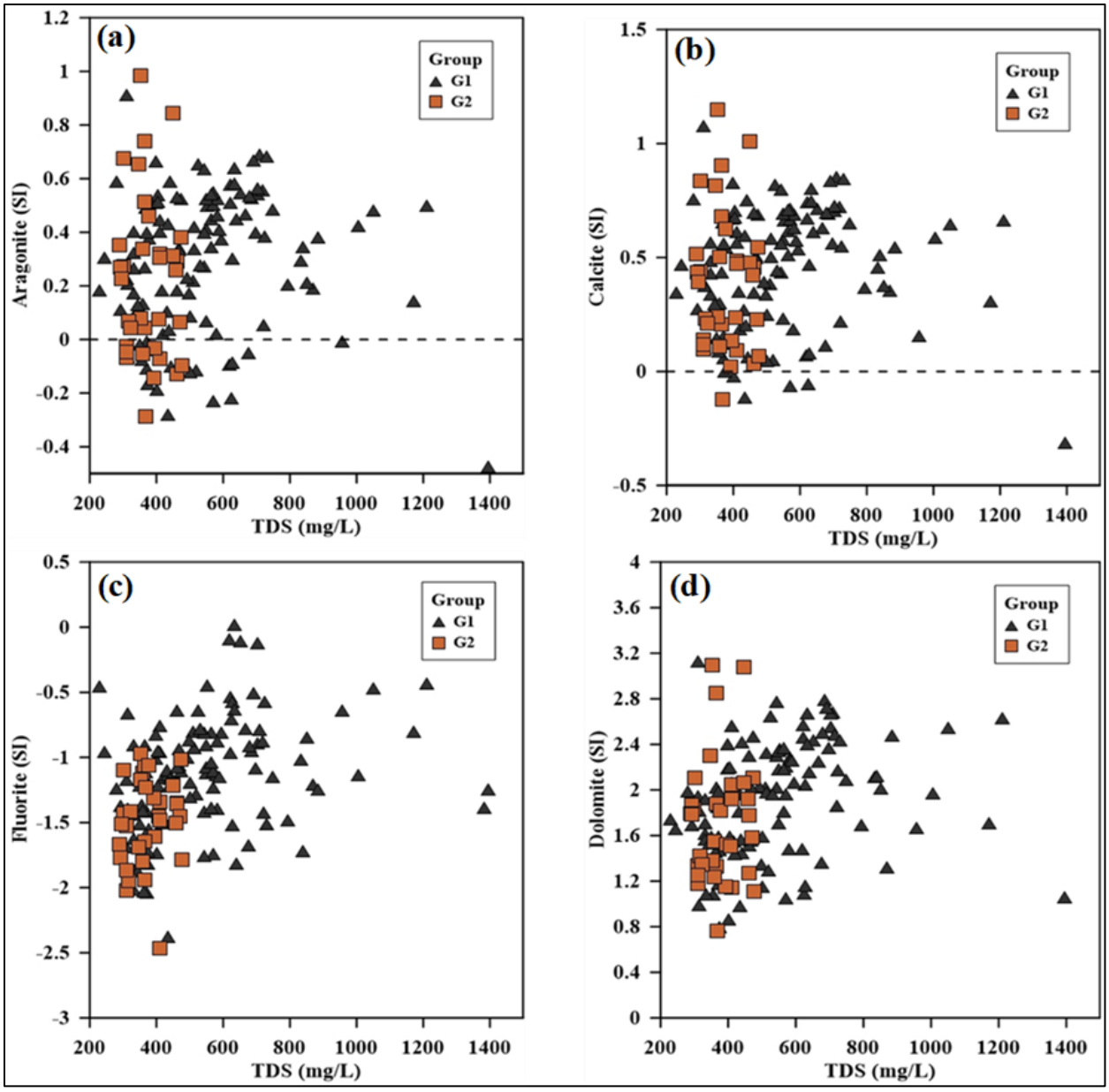


**Figure 4.11**: Mineral saturation indices calculated for (a) aragonite (b) calcite (c) fluorite, and (d) dolomite

The $Ca^{2+}$ + $Mg^{2+}$ versus $HCO_3^-$ plot (Figure 4.12d) suggests contributions from both silicate and carbonate weathering processes, as evidenced by some groundwater samples aligning with the 1:1 line (Datta and Tyagi, 1996; Masoud et al., 2018; Kumar et al., 2021). However, the excess $HCO_3^-$ relative to $Ca^{2+}$ indicates additional cation sources, likely from silicate weathering and the

dissolution of sodic soils, as observed in both groups of samples. The chemical weathering of these minerals significantly increases the concentration of various ions in the groundwater.

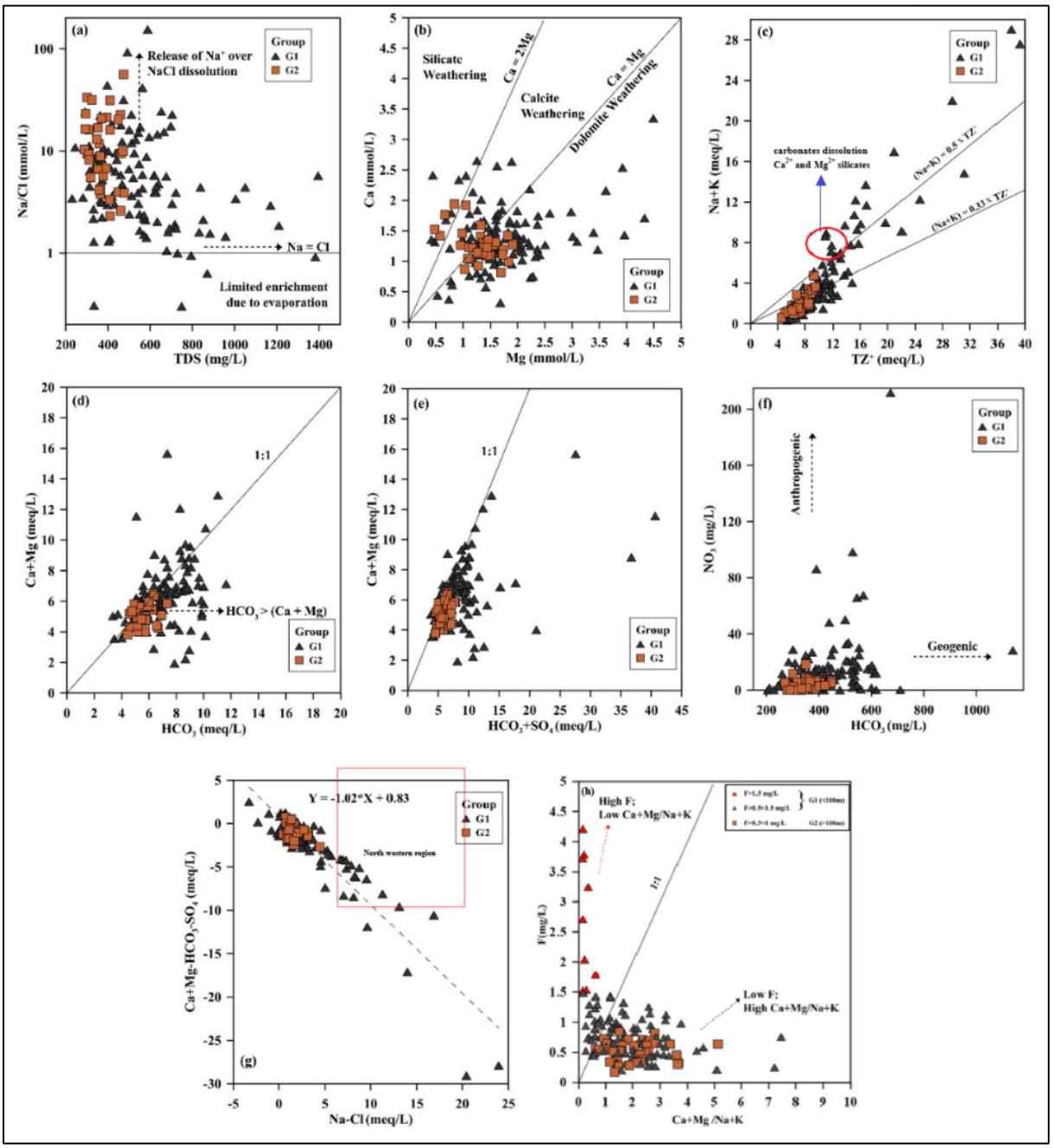


**Figure 4.12**: (a) TDS vs Na+/Cl- (b) $Ca^{2+}$ vs $Mg^{2+}$ (c) $TZ^{+}$ vs $Na^{+}$+$K^{+}$ (d) $HCO_3^{-}$ vs $Ca^{2+}$+$Mg^{2+}$ (e) $SO_4^{2-}$+$HCO_3^{-}$ vs $Mg^{2+}$+$Ca^{2+}$ (f) $HCO_3^{-}$ vs $NO_3^{-}$ (g) $Na^{+}$-$Cl^{-}$ vs $Ca^{2+}$+$Mg^{2+}$-$HCO_3^{-}$ -$SO_4^{2-}$, and (h) $Ca^{2+}$+$Mg^{2+}$/ $Na^{+}$+$K^{+}$ vs $F^{-}$

Figure 4.12e highlights the importance of ion exchange and reverse ion exchange processes in shaping groundwater chemistry. Samples aligning with the 1:1 line are primarily influenced by silicate and carbonate weathering. However, an excess of sulfate and bicarbonate ions ($SO_4^{2-}$ + $HCO_3^-$) suggests additional cation sources from silicate weathering or ion exchange, particularly evident in the G2 group. Conversely, elevated calcium and magnesium levels in some G1 and G2 samples indicate carbonate weathering or reverse ion exchange. To accurately assess the contribution of ion exchange, it is crucial to account for other processes like silicate and carbonate weathering, as genetically related cations should balance each other.

Figure 4.12g demonstrates a strong correlation between cation and anion exchange, indicating the dominance of ion exchange processes in the aquifer system. While most samples exhibit typical ion exchange behavior, some G1 group samples suggest reverse ion exchange. Deeper groundwater samples (G2 group) cluster near the origin, indicating a sand-dominated environment with limited clay minerals and, consequently, fewer ion exchange sites at depths greater than 100-210 meters.

The majority of nitrate-enriched groundwater samples (75%) originate from agricultural fields, while the remaining 25% are sourced from human settlements. This suggests that excessive use of chemical fertilizers in agricultural areas, along with domestic waste and leaky septic tanks in human settlements, are the primary causes of local groundwater nitrate contamination. These factors, however, have a less significant impact on a larger scale (Hudak, 1999).

The northwestern region of the study area is characterized by high $F^-$ concentrations in the G1 group groundwater samples, with a maximum concentration of 4.21 mg/l (Table 4.1). This region also exhibits sodic water types and alkaline conditions, which facilitate $F^-$ mobilization from the soil or aquifer matrix. The plot of $F^-$ vs. $(Ca^{2+} + Mg^{2+})/(Na^+ + K^+)$ (Figure 4.12h) indicates that ion exchange processes and silicate mineral weathering under alkaline conditions are responsible for the fluoride-rich groundwater (Patel et al., 2024).

**Therefore, in the study area, groundwater chemistry is influenced by both silicate and carbonate weathering, with a localized nitrate contamination issue attributed to human activities.**

### 4.3.4 Non-Carcinogenic Health Risk Assessment due to Fluoride and Nitrate

Humans are primarily exposed to fluoride and nitrate health risks through prolonged oral consumption of contaminated water. The non-carcinogenic health risk associated with $F^-$ and $NO_3^-$ was assessed using the Hazard Quotient (HQ), where an HQ greater than 1 indicates a potential non-carcinogenic risk. The spatial distribution of the calculated HQ values is represented as a bubble plot (Figure 4.13a-b).

An HQ > 1 for $F^-$ is observed in the northwestern and southeastern regions, consistent with areas where $F^-$ concentrations exceed 1.5 mg/l. Additionally, two groundwater samples with HQ > 1 were identified in the southern region. For nitrate, only groundwater samples from agricultural fields exceeded the HQ >1 threshold.

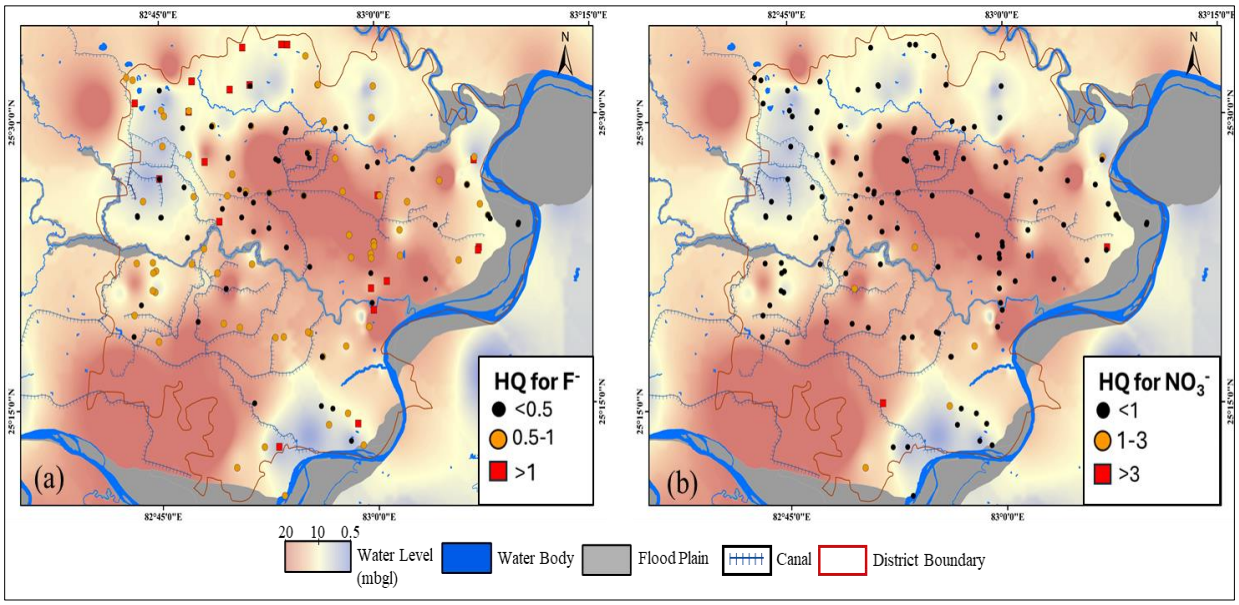


**Figure 4.13**: (a) Hazard Quotient (HQ) plotted as bubble plot for $F^-$, (b) Hazard Quotient (HQ) plotted for $NO_3^-$

**Based on the current groundwater data, fluoride contamination appears to be more widespread than nitrate, emphasizing the need for targeted on-site mitigation measures.**

## 4.4 Trace metal concentration in groundwater (2021-2022)

Approximately 150 groundwater samples were analyzed across two phases. In 2021, 80 samples were tested for 11 trace metals, while in 2022, 76 samples were analyzed for 21 trace metals. Eleven trace metals (Al, Cr, Mn, Fe, Co, Ni, Cu, Zn, As, Cd, Pb) were common to both years. Additionally, 10 trace metals (Be, B, V, Se, Sr, Ba, Ce, Hg, Th, U) were analyzed during the post-monsoon season of 2022. The occurrence and distribution of these trace metals in the groundwater of the study area are discussed in the following sections. Among the 11 trace metals analyzed (2021) the mean abundance follows an order of Zn>Fe>Al>Mn>Cu>As>Cr>Ni>Pb>Co>Cd.

**Table 4.3**: Descriptive statistics showing Trace Metal concentrations in groundwater along with various significant Physico-Chemical parameters (2021)

| Parameter | Mean | Min | Max | Std. Dev | Skewness | BIS (2012) | No. of samples | % Samples exceeding |
|---|---|---|---|---|---|---|---|---|
| BD (m) | 66.2 | 2.2 | 213.4 | 46 | 0.9 | | | |
| pH | 7.5 | 7 | 8.3 | 0.3 | 0.7 | | | |
| EC (µS/cm) | 900.5 | 325 | 2630 | 386.4 | 2 | | | |
| Temp (°C) | 26.6 | 22.4 | 30 | 1.1 | -0.4 | | | |
| Al (µg/l) | 14.3 | BDL | 416.3 | 46.7 | 6.1 | 30 | 13 | 8.5 |
| Cr (µg/l) | 0.7 | BDL | 6 | 0.9 | 2.4 | 50 | | |
| Mn (µg/l) | 4.8 | BDL | 109.8 | 13.5 | 5.2 | 100 | 1 | 0.7 |
| Fe (µg/l) | 38.2 | BDL | 1322 | 149.6 | 6.5 | 300 | 6 | 3.9 |
| Co (µg/l) | 0.1 | BDL | 0.8 | 0.1 | 4.2 | | | |
| Ni (µg/l) | 0.3 | BDL | 3 | 0.5 | 2.8 | 20 | | |
| Cu (µg/l) | 2.1 | BDL | 40.1 | 5 | 5.3 | 50 | | |
| Zn (µg/l) | 91.3 | BDL | 1800 | 233 | 4.3 | 5000 | | |
| As (µg/l) | 0.9 | BDL | 5.1 | 0.9 | 1.9 | 10 | | |
| Cd (µg/l) | 0 | BDL | 0.7 | 0.1 | 9.4 | 3 | | |
| Pb (µg/l) | 0.2 | BDL | 3.1 | 0.4 | 3.9 | 10 | | |

BDL (below detection limit)

1. **Aluminum**: In the study area, $Al^{3+}$ concentration ranges from BDL to 416.3(±46.7), with an average value of 14.3, with 13 samples exceeding the recommended value of 30 µg/l (Table 4.3). Aluminum occurs in many silicate minerals such as micas, amphiboles, and feldspar, and forms the basic unit structure in these silicate minerals.

2. **Manganese**: The manganese concentration in groundwater ranges from below detection limits (BDL) to 109.8 µg/l, with an average of 4.8 ± 13.5 µg/l. One sample exceeds the recommended limit of 100 µg/l set by BIS (2012), while three samples surpass the USEPA (2018) guideline of 50 µg/l. Prolonged exposure to elevated $Mn^{2+}$ levels in drinking water can affect children's learning abilities and cause cosmetic effects such as skin discoloration. Additionally, changes in taste, odor, and water color may also occur (WHO, 2017).

3. **Iron**: The total iron (Fe) concentration in the groundwater samples varied significantly, ranging from below detection limits (BDL) to a high of 1322.4 µg/L. The average Fe concentration was 38.2 µg/L, with a high standard deviation of 149.6 µg/L, indicating substantial spatial variability in Fe levels. Six samples exceeded the recommended limit of 300 µg/L, all of which were from India Mark II hand pumps tapping the shallow first aquifer at depths of up to 150 meters below ground level (m bgl). The elevated Fe concentrations are primarily attributed to geogenic sources, such as the weathering of silicate minerals like pyroxenes, amphiboles, and biotite. Additionally, sedimentary minerals containing iron, including siderite (FeCO3), ferric oxide and hydroxide nodules (hematite), and goethite (FeOOH), which are commonly found in the uppermost soil layers throughout the study area.

4. **Arsenic**: In the present study, most of the groundwater samples are sampled from the older alluvium, and no groundwater sample has exceeded the recommended value of 10 µg/l.

5. **Uranium:** Groundwater uranium concentrations ranged from 0.96 to 86.2 µg/L, with an average of 16.4 µg/L and a standard deviation of 18.3 µg/L. Thirteen out of 76 groundwater samples exceeded the World Health Organization (WHO, 2017) guideline value of 30 µg/L. All contaminated samples were sourced from the first aquifer between the surface and 150 meters below ground level (m bgl) and within 60 meters of the water table. The presence of

granitic minerals like feldspar, mica, and amphibole in the soil, when leached, can elevate uranium concentrations in groundwater. Additionally, uranium-containing phosphate fertilizers can contribute to groundwater contamination, particularly in shallow aquifers.

**Table 4.4**: Descriptive statistics showing Trace Metal concentrations in groundwater (2022)

| Parameter | Mean | Min | Max | Std. Dev | Skewness | BIS (2012) | no. of samples | % Samples exceeding |
|---|---|---|---|---|---|---|---|---|
| Be | 0.01 | 0.00 | 0.1 | 0.0 | 4.4 | 4 | | |
| B | 94.80 | 17.11 | 882.7 | 137.8 | 3.7 | 500 | 2 | 2.6 |
| V | 3.45 | 0.04 | 14.2 | 2.2 | 2.3 | | | |
| Se | 0.71 | 0.00 | 4.9 | 1.1 | 2.3 | 10 | | |
| Sr | 611.91 | 58.74 | 3981.9 | 577.6 | 3.9 | 4000 | | |
| Ba | 45.38 | 5.90 | 183.3 | 40.0 | 1.7 | 700 | | |
| Ce | 0.01 | BDL | 0.0 | 0.0 | 2.6 | | | |
| Hg | 0.03 | BDL | 0.2 | 0.0 | 1.7 | 1 | | |
| Th | 0.02 | BDL | 0.1 | 0.0 | 2.8 | | | |
| U | 16.47 | 0.96 | 86.2 | 18.3 | 2.2 | 30 | 13 | 17.1 |

6. **Boron:** The boron concentration in the groundwater samples varied significantly, ranging from a low of 17.11 µg/L to a high of 882.7 µg/L. The average boron concentration was 94.80 µg/L, with a standard deviation of 137.8 µg/L, indicating substantial variability in boron levels across the samples. Two groundwater samples exceeded the World Health Organization (WHO, 2017) recommended limit of 500 µg/L.

### 4.4.1 Spatial variability of selected trace metals in groundwater

Among the eleven trace metals analyzed in the groundwater samples (2021), spatial variability was observed for four: iron, aluminum, manganese, and arsenic. **Iron:** Four groundwater samples exceeded the permissible limit of 300 µg/L, primarily from the eastern side of the district and shallow groundwater systems. **Aluminum:** Thirteen samples exceeded the permissible limit of

aluminum. These were mostly from shallow depths in the eastern and southeastern regions. The acidic hydrolysis of aluminosilicates in the alluvial setting likely contributed to elevated aluminum concentrations in shallow groundwater. **Manganese:** Only one sample, located in the northeast and sourced from an Indian Mark II hand pump, exceeded the permissible limit of 30 µg/L for manganese. **Arsenic:** No groundwater samples exceeded the permissible limit of 10 µg/L for arsenic. The older, oxidized alluvium in the region is generally not conducive to arsenic enrichment in groundwater (Mukherjee et al., 2024).

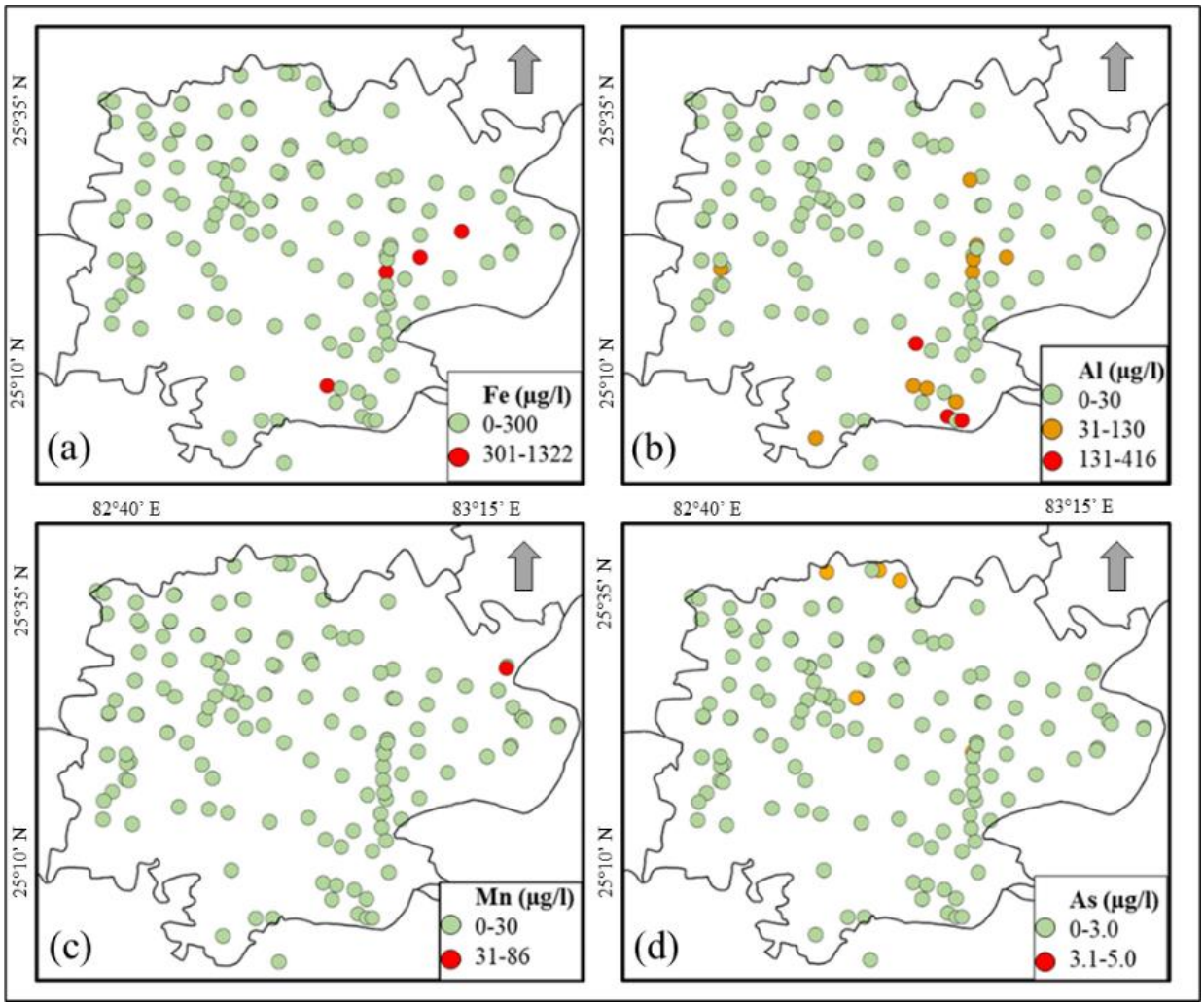


**Figure 4.14**: Spatial variability maps (a) total iron ($Fe^{2+}$ & $Fe^{3+}$) in groundwater, (b) aluminium ($Al^{3+}$), (c) Manganese ($Mn^{2+}$), (d) total arsenic in groundwater ($As^{3+}$ & $As^{5+}$)

## 4.5 Results of Environmental isotopes

The various isotopes analyzed in groundwater, surface water and rainwater have been reported in the following section to decipher the recharge sources and zones of the aquifer system, understanding the surface water- groundwater interactions and interconnection of aquifers.

### 4.5.1 $\delta^{18}O$ and $\delta^{2}H$ composition of rainfall

The stable isotope composition of the rainfall samples varied significantly. The $\delta^{18}O$ values ranged from -14.6‰ to 1.4‰, while $\delta^{2}H$ values ranged from -104.9‰ to 14.7‰. The d-excess values, which represent the deviation from the Global Meteoric Water Line (GMWL), ranged from 2‰ to 20‰. For the present study, the corresponding d-excess and EC values vary from 8‰ to 16‰ (avg: 11‰) and µS/cm (avg: 10µS/cm), respectively. The average d-excess value 10 ‰ is the same as of average global 10‰. This reflects impact of south-west monsoon which contributes more than 85% of rainfall in the current area, and peak time for groundwater infiltration and aquifer recharge (Dey et al., 2020; Das et al., 2021).

Seasonal variations were observed in the $\delta^{18}O$ values, with post-monsoon rains being more depleted than monsoon and pre-monsoon events. The d-excess values also varied seasonally, with pre-monsoon, monsoon, and post-monsoon/winter having mean values of 7‰, 10‰, and 15‰, respectively. These variations in d-excess are likely due to differences in the original moisture source. Additionally, a relationship between rainfall amount and isotopic composition was observed. Heavier rainfall events were generally more depleted in $\delta^{18}O$ compared to lighter events. This is attributed to the amount effect, where heavier isotopes tend to be preferentially incorporated into the liquid phase during precipitation.

**Table 4.5**: Descriptive statistics of rainfall (n=60) of Varanasi district collected from BHU station

| Statistics | $\delta^{18}O$ (‰) | $\delta^{2}H$ (‰) | d-excess | Amount (mm) |
|---|---|---|---|---|
| min | -14.6 | -104.9 | 2 | 0.2 |
| max | 1.4 | 14.7 | 20 | 106 |
| average | -7.7 | -51.9 | 10 | 23.5 |

### 4.5.2 Development of Local Meteoric water line (LMWL)

In this study, the isotopic composition of oxygen ($\delta^{18}O$) and hydrogen ($\delta^{2}H$) in 60 rainfall samples was analyzed to establish a Local Meteoric Water Line (LMWL) specific to Varanasi. The LMWL was then compared to the Global Meteoric Water Line (GMWL) defined by Rozanski et al. (1993) and the Indian Meteoric Water Line (IMWL) developed by Kumar et al. (2010).

$$\text{LMWL; } \delta^{2}H = 7.5(\pm 0.1) \times \delta^{18}O + 5.9(\pm 0.6); \ (R^2 = 0.99, p<0.01)$$

The developed Local Meteoric Water Line (LMWL) is parallel to the Global Meteoric Water Line (GMWL) and the Indian Meteoric Water Line (IMWL), but it has a lower slope and intercept compared to both. Since average rainfall values can be skewed, the Annual Weighted Average Precipitation (AWAP) was calculated by multiplying each $\delta^{18}O‰$ value of rainfall by its corresponding rainfall amount and dividing it by the total rainfall amount.

For the present study, the AWAP value across all seasons is -8.1‰ ($\delta^{18}O$) (Figure 6.5a), while for the monsoon season, it is -7.0‰ ($\delta^{18}O$) (Figure 6.5b). The lower slope and intercept of the precipitation line (LMWL) compared to the GWML and IMWL can be attributed to the prolonged travel of the original moisture source (continental effect) and subsequent rain-out processes during its trajectory (Dansgaard, 1964; Kumar et al., 2010).

### 4.5.3 $\delta^{18}O$ and $\delta^{2}H$ composition of surface water

A total of 19 surface water samples were analyzed for isotopic characterization, including 10 Ganga River samples from Rai et al. (2021) and 9 samples from the present study (Figure 6). The $\delta^{18}O$ values for the Ganga River samples range from -8.1‰ to -4.9‰, with an average of -6.6‰ (±0.7‰), while $\delta^{2}H$ values range from -55.1‰ to -38.0‰, with an average of -47.6‰ (±4.7‰). The corresponding d-excess values vary from 1‰ to 11‰, with an average of 6‰ (±3‰) (Table 4.6).

The $\delta^{18}O$ and $\delta^{2}H$ values for the Ganga River samples generally align with the Local Meteoric Water Line (LMWL), with a few falling slightly below it. Samples on the meteoric water line, closely approximating the AWAP, indicate that local precipitation significantly contributes to the

river discharge (Figure 4.15). However, some samples with depleted isotopic signatures compared to local precipitation suggest contributions from upstream recharge in the Ganga, potentially from the Himalayas.

For the pond sample, the $\delta^{18}O$ and $\delta^{2}H$ values are -7.9‰ and -55‰, respectively. Similarly, the canal samples collected during the post-monsoon season exhibit $\delta^{18}O$ and $\delta^{2}H$ values of -7.4‰ and -50‰, respectively. The isotopic composition of the canal water reflects the characteristics of the Ganga River, as the canal carries Ganga water.

Ganga River; $\delta^{2}H = 7.2 \times \delta^{18}O + 0.19$

**Table 4.6**: Descriptive statistics of stable isotopic signatures of Ganga River

| Parameter | Min | Max | Mean | Std. Dev | Skewness |
|---|---|---|---|---|---|
| $\delta^{18}O$‰ | -8.1 | -4.9 | -6.6 | 0.7 | 0.5 |
| $\delta^{2}H$‰ | -55.1 | -38.0 | -47.6 | 4.7 | 0.4 |
| d-excess | 1 | 10 | 6 | 3 | -0.1 |

### 4.5.4 $\delta^{18}O$ and $\delta^{2}H$ composition of Groundwater

Groundwater samples collected from various borehole depths across the Varanasi district were analyzed for stable isotopes ($\delta^{18}O$ and $\delta^{2}H$). The $\delta^{18}O$ values range from -7.72‰ to -4.92‰, with an average of -6.22‰ (±0.59‰), while $\delta^{2}H$ values range from -54.89‰ to -38.62‰, with an average of -45.77‰ (±3.5‰). The corresponding d-excess values range from 1‰ to 9‰, with an average of 5‰ (±2‰) (Table 4.7). Similar variability was observed in electrical conductivity (EC) and other ions. The EC values range from 420 µS/cm to 2630 µS/cm, with a mean of 793 µS/cm (±307.7 µS/cm).

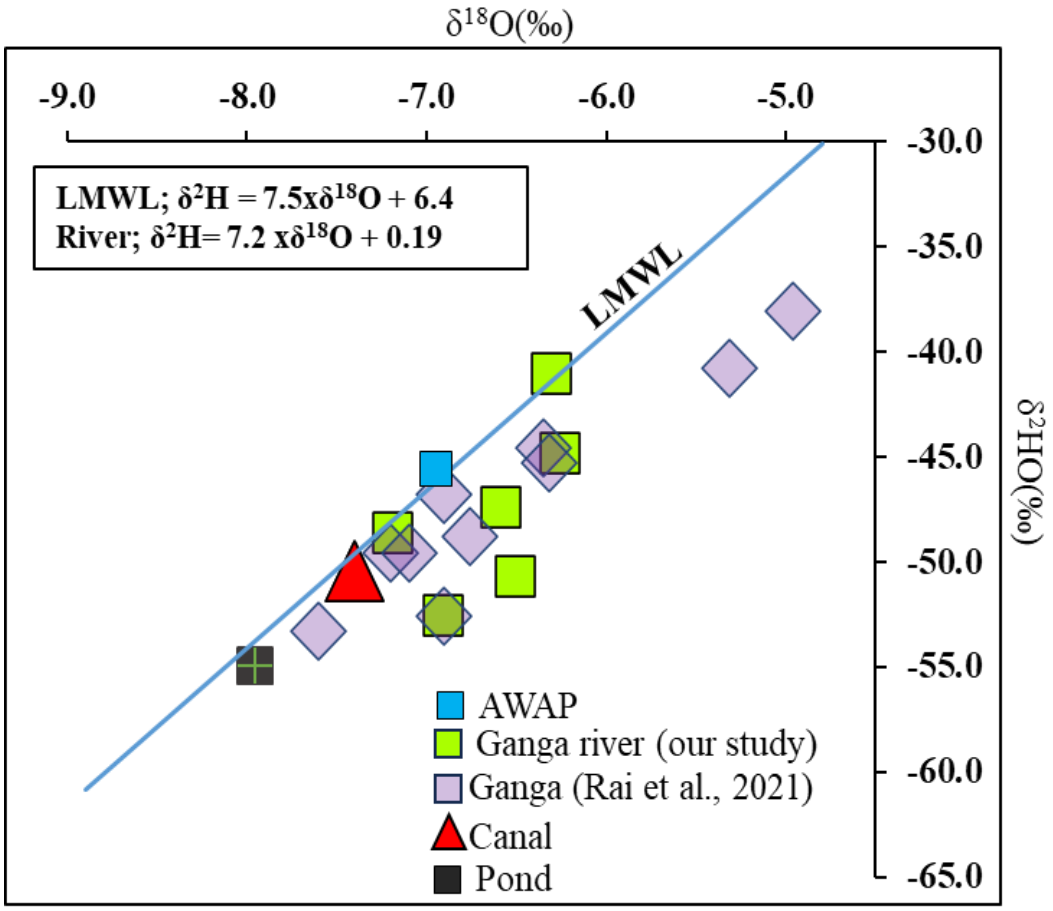


**Figure 4.15:** The cross-plot of $\delta^{18}O$ and $\delta^{2}H$ for surface water samples distinguishes various water sources using specific markers.

**Table 4.7**: Descriptive statistics of groundwater samples collected for the stable isotopes across different borewell depth

| Parameter | BD(m) | pH | EC (µS/cm) | $\delta^{18}O$‰ | $\delta^{2}H$‰ | d- excess ‰ |
|---|---|---|---|---|---|---|
| min | 40 | 6.40 | 420 | -7.72 | -54.89 | 1 |
| max | 213.3 | 8.40 | 2630 | -4.92 | -38.62 | 9 |
| mean | 76.8 | 7.21 | 793 | -6.22 | -45.77 | 5 |
| median | 69.8 | 7.25 | 712 | -6.15 | -45.53 | 5 |
| Std. Dev | 48.8 | 0.35 | 306 | 0.59 | 3.53 | 2 |

Similar to groundwater hydrochemical evolution, the stable isotopic composition of groundwater also varies with depth (Figure 4.16a). Groundwater samples collected from depths up to 100 m below ground level (bgl) exhibit $\delta^{18}O$ values ranging from -7.3‰ to -4.9‰, with an average of -6.1‰, and $\delta^{2}H$ values ranging from -51.7‰ to -38.6‰, with an average of -45.4‰. The corresponding d-excess values range from 1‰ to 8‰, with an average of 5‰, while electrical conductivity (EC) varies from 437 µS/cm to 2630 µS/cm, with an average of 822 µS/cm (Figure 4.16b).

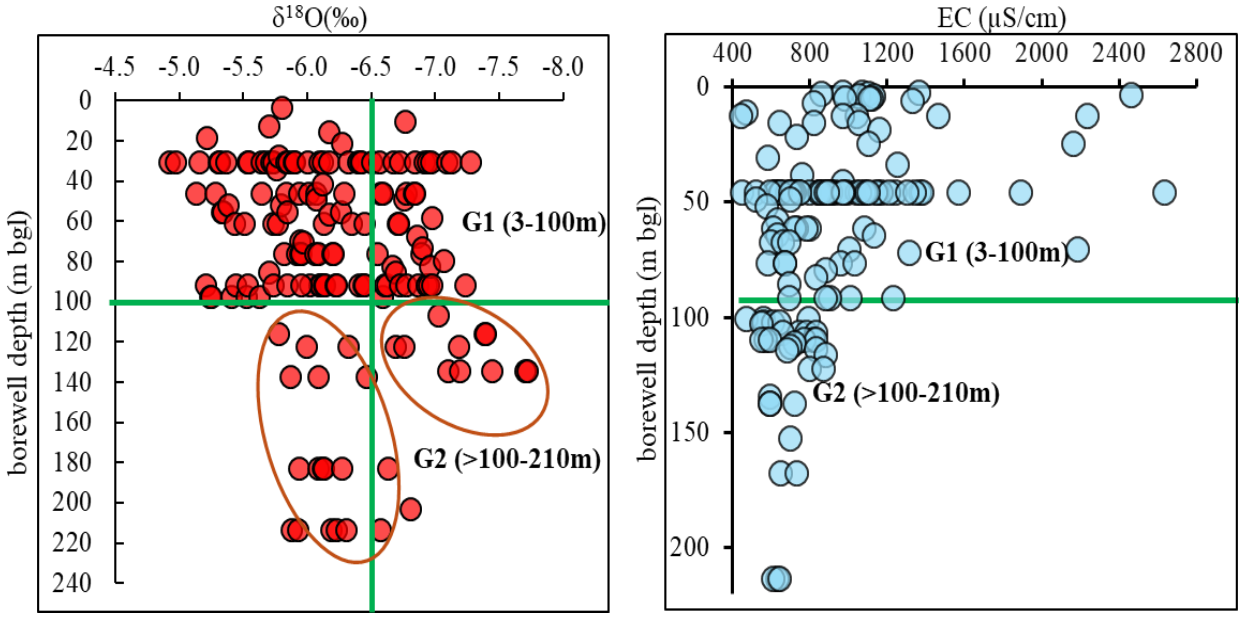


**Figure 4.16**: The plot between $\delta^{18}O$ vs borewell depth (in red circle) and the corresponding EC vs Borewell depth (in blue circle) represents vertical variation.

This large variation in isotopic signatures up to 100 m depth aligns with the hydrochemical characteristics of the G1 group and indicates multiple recharge sources (Patel et al., 2024). In contrast, groundwater samples from depths greater than 100 m bgl (G2 group) show reduced variability in isotopic composition. $\delta^{18}O$ values range from -7.7‰ to -5.8‰, with an average of -6.6‰, while $\delta^{2}H$ values range from -54.9‰ to -42.6‰, with an average of -47.5‰. The d-excess values for this group range from 4‰ to 9‰, with an average of 6‰.

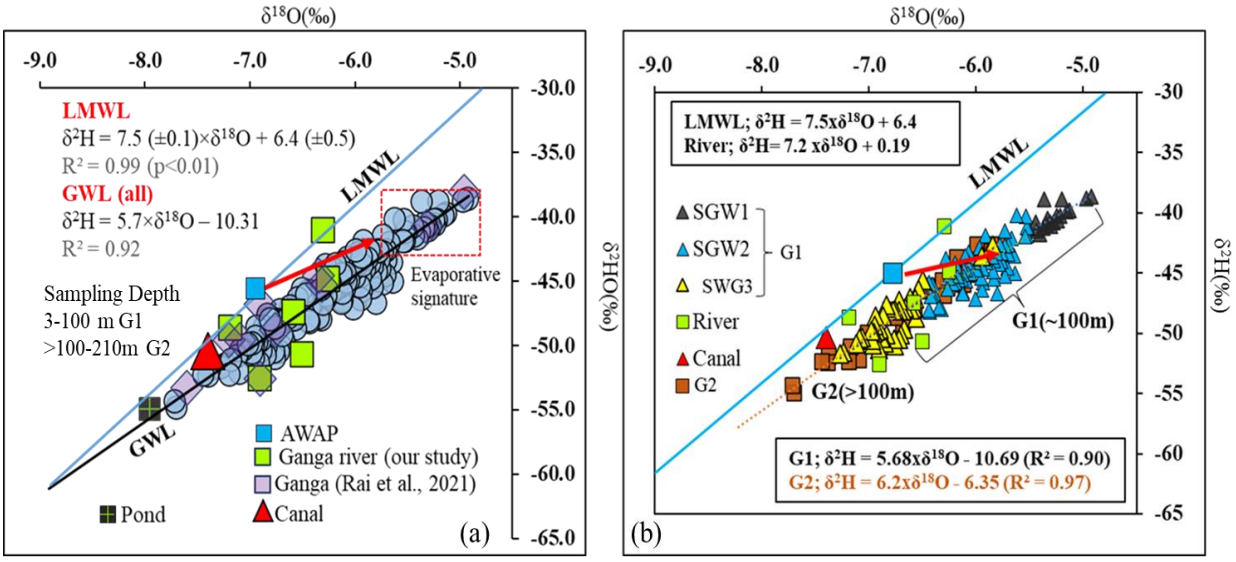


**Figure 4.17**: (a) Cross plot between $\delta^{18}O$and $\delta^{2}H$ of groundwater samples, sky solid line corresponds to LMWL, and black solid line corresponds to groundwater line, (b) groundwater samples from group G1 (3-100m) were further classified to SGW1(black triangle), SGW2(blue triangle), and SGW3(yellow triangle).

**Table 4.8**: Descriptive statistics of stable isotopic signature for G1 group samples (up to 100m) & G2 (100 to 210 m (maximum sampling depth)

| G1 | Min | Max | Mean | Std. Dev | G2 | Min | Max | Mean | Std. Dev |
|---|---|---|---|---|---|---|---|---|---|
| BD (m) | 3.0 | 97.5 | 57.6 | 26.4 | BD(m) | 106.7 | 213.4 | 157.5 | 38.4 |
| EC (µS/cm) | 437.0 | 2630.0 | 822.3 | 332.2 | EC (µS/cm) | 420.0 | 880.0 | 670.3 | 105.3 |
| δ18O | -7.27 | -4.92 | -6.14 | 0.57 | δ18O | -7.70 | -5.80 | -6.57 | 0.59 |
| δ2H | -51.72 | -38.62 | -45.36 | 3.37 | δ2H | -54.90 | -42.60 | -47.49 | 3.78 |
| d-excess | 1 | 8 | 5 | 2 | d-excess | 4 | 9 | 6 | 1 |

The attenuation of isotopic values below 100 m bgl indicates greater consistency in recharge sources. The observed isotopic variations align with the hydrochemical characteristics of groundwater, which have been categorized into two groups: G1 (<100 m bgl) and G2 (>100 m bgl). The regression equations for the two groups are as follows:

- **Group G1 (samples up to 100 m bgl):** G1; $\delta^2H = 5.68(\pm 0.17) \times \delta^{18}O - 10.69(\pm 1.05)$ ($R^2 = 0.89$, $p<0.01$)
- **Group G2 (samples >100 m bgl):** G2; $\delta^2H = 6.2(\pm 0.22) \times \delta^{18}O - 6.35(\pm 1.4)$ ($R^2 = 0.97$, $p<0.01$)

### 4.5.5 Spatial variability of $\delta^{18}O$, d-excess of groundwater

The $\delta^{18}O$ values of the G1 group groundwater samples exhibit relatively enriched signatures (-4.9‰ to -6.0‰) in the northwestern, northern, and southeastern urban regions. In contrast, comparatively depleted values (-6.1‰ to -7.1‰) are observed across the central stretch of the study area, extending from west to east (Figure 4.18).

For the G2 group groundwater samples (100–210 m bgl), represented as red bubbles in the plot, $\delta^{18}O$ values show more depleted signatures (-6.5‰ to -7.7‰) predominantly in the southeastern region. However, relatively enriched $\delta^{18}O$ values (-5.8‰ to -6.4‰) are observed at a few locations in the northern and eastern parts of the study area.

The spatial variability map of d-excess for G1 group groundwater samples reveals that the central, eastern, western, and southern regions exhibit relatively higher d-excess values (6‰ to 8‰), whereas lower d-excess values are observed in the northwestern and southeastern regions. This trend is inversely related to the spatial patterns of $\delta^{18}O$ and $\delta^2H$ values.

Groundwater with higher d-excess values in the study area suggests minimal fractionation during recharge, indicating rapid recharge processes. Conversely, lower d-excess values point to recharge from a more evaporative source, where greater isotopic fractionation has occurred (Figure 4.19).

These findings suggest that recharge occurs more quickly in the central part of the study area compared to other regions.

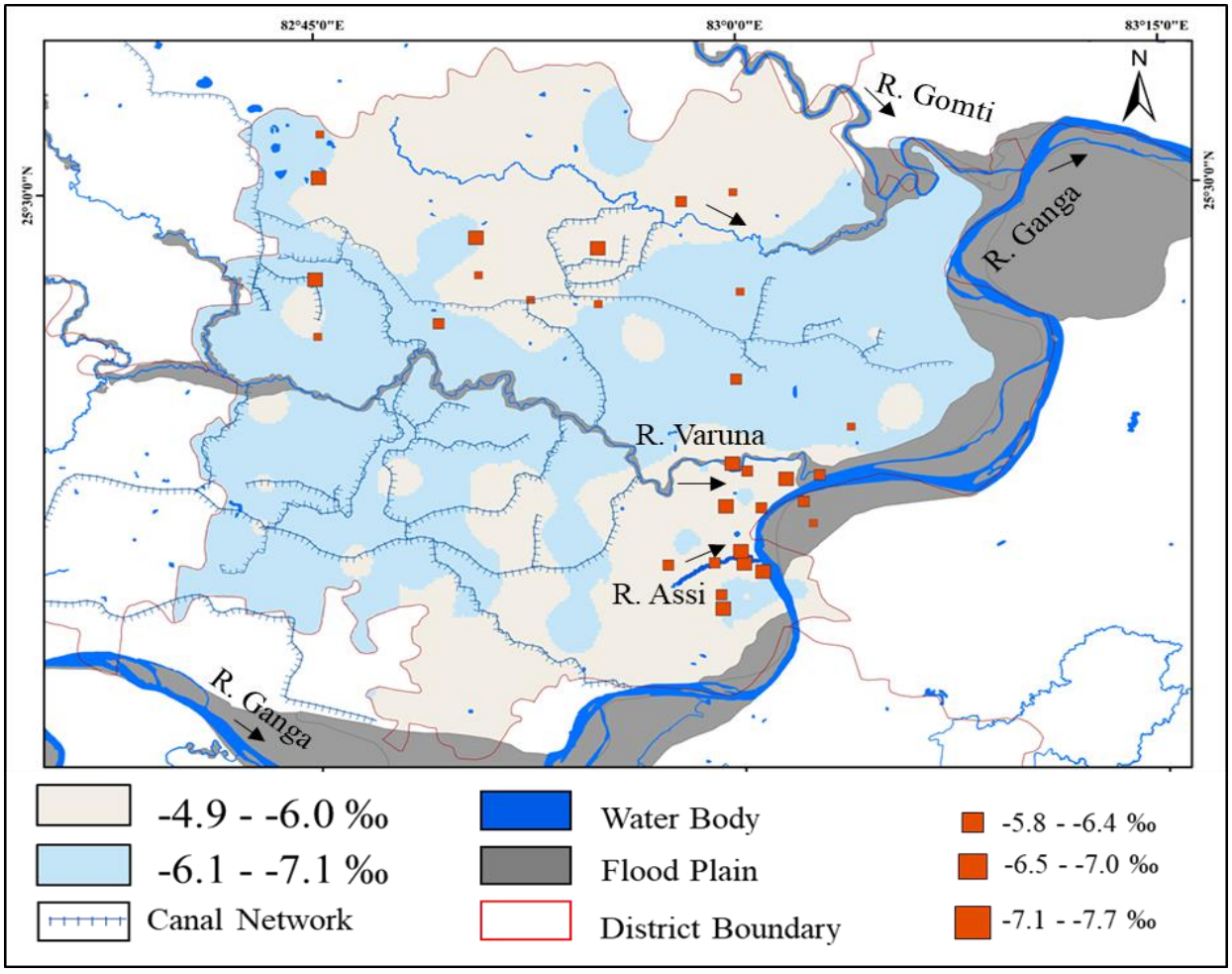


**Figure 4.18**: Spatial variability of map of $\delta^{18}O$ for both the groups along with canal networks, and major drainage of the study area.

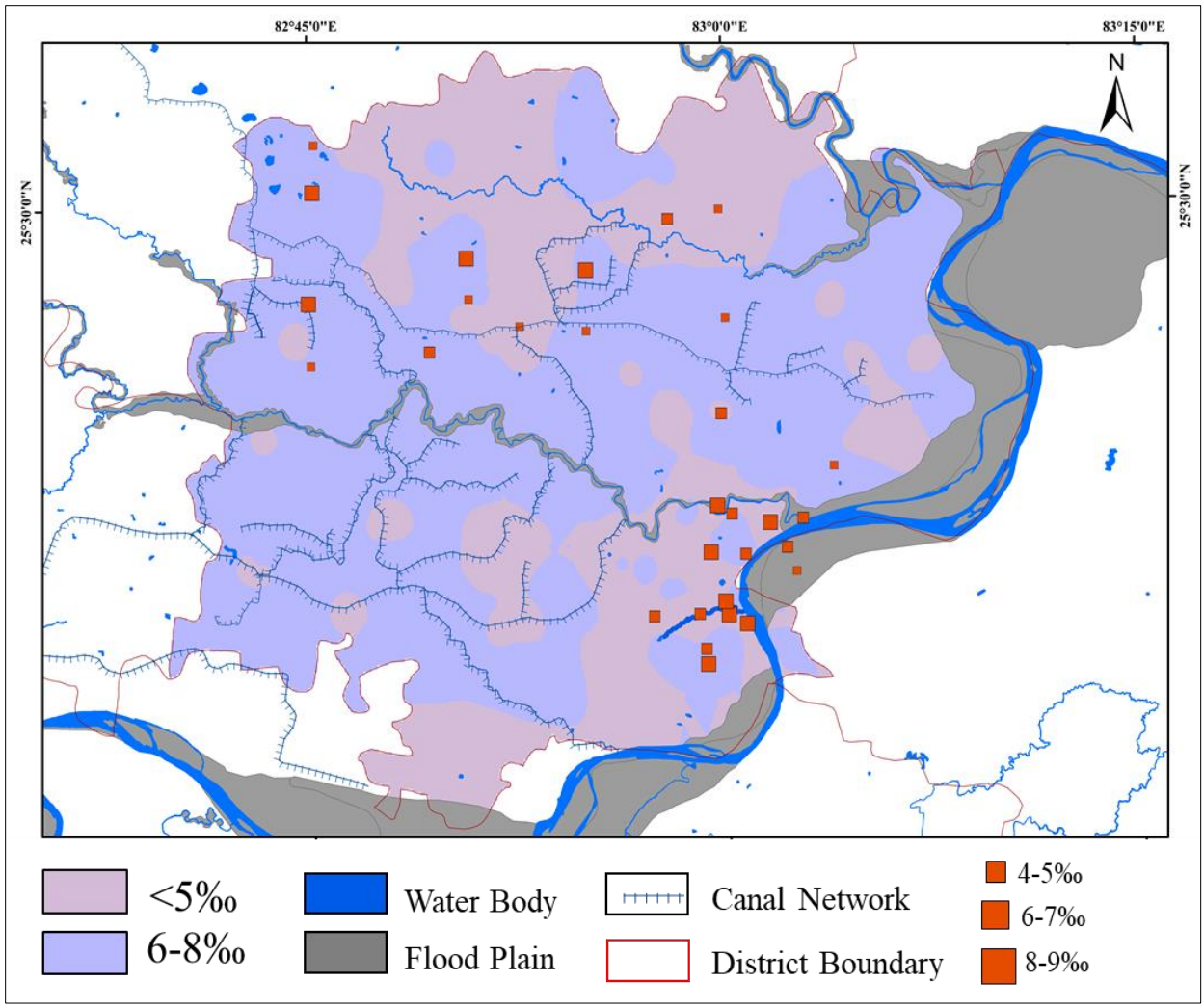


**Figure 4.19**: Spatial variability of map of d-excess for both the groups along with canal networks, and major drainage of the study area.

### 4.5.6 Tracing recharge sources and zones of Groundwater

The significant variation in $\delta^{18}O$ and $\delta^{2}H$ values in groundwater can be attributed to multiple factors, including recharge sources, the subsurface framework of the area, the presence of surface water bodies (e.g., rivers, canals, irrigation returns, ponds, lakes), anthropogenic activities, and the depth of water samples (Das et al., 2021; Patel et al., 2024).

To better understand the recharge processes dominating up to 100 m bgl (i.e., G1 group), several analytical tools were utilized: the $\delta^{18}O$ vs $\delta^{2}H$ cross plot, spatial variability maps of $\delta^{18}O$, and d-

excess, and subsurface lithology. Together, these provide insights into the interplay of various recharge mechanisms and the controlling factors in the study area. Due to large variation $\delta^{18}O$ and $\delta^{2}H$ values in the groundwater of the G1 group is further subdivided into three subgroups SGW1, SGW2, and SGW3 (Table 4.9).

Table 4.9: Descriptive statistics of stable isotopic signature for SGW1, SGW2 and SGW3

| | **SGW1** | | | **SGW2** | | | **SGW3** | | |
|---|---|---|---|---|---|---|---|---|---|
| **Parameter** | **Min** | **Max** | **Mean** | **Min** | **Max** | **Mean** | **Min** | **Max** | **Mean** |
| BD(m) | 18.3 | 97.5 | 55.0 | 3.0 | 97.5 | 55.8 | 10.0 | 97.5 | 61.6 |
| EC (µS/cm) | 580.0 | 2230.0 | 829.0 | 437.0 | 2630.0 | 830.2 | 470.0 | 2180.0 | 806.6 |
| δ18O ‰ | -5.4 | -4.9 | -5.3 | -6.4 | -5.5 | -6.0 | -7.3 | -5.8 | -6.8 |
| δ2H ‰ | -41.7 | -38.6 | -40.3 | -48.2 | -40.2 | -44.6 | -51.7 | -42.7 | -48.9 |
| d-excess | 1.6 | 5.0 | 2.7 | 0.7 | 7.5 | 4.3 | 4.2 | 8.2 | 6.4 |

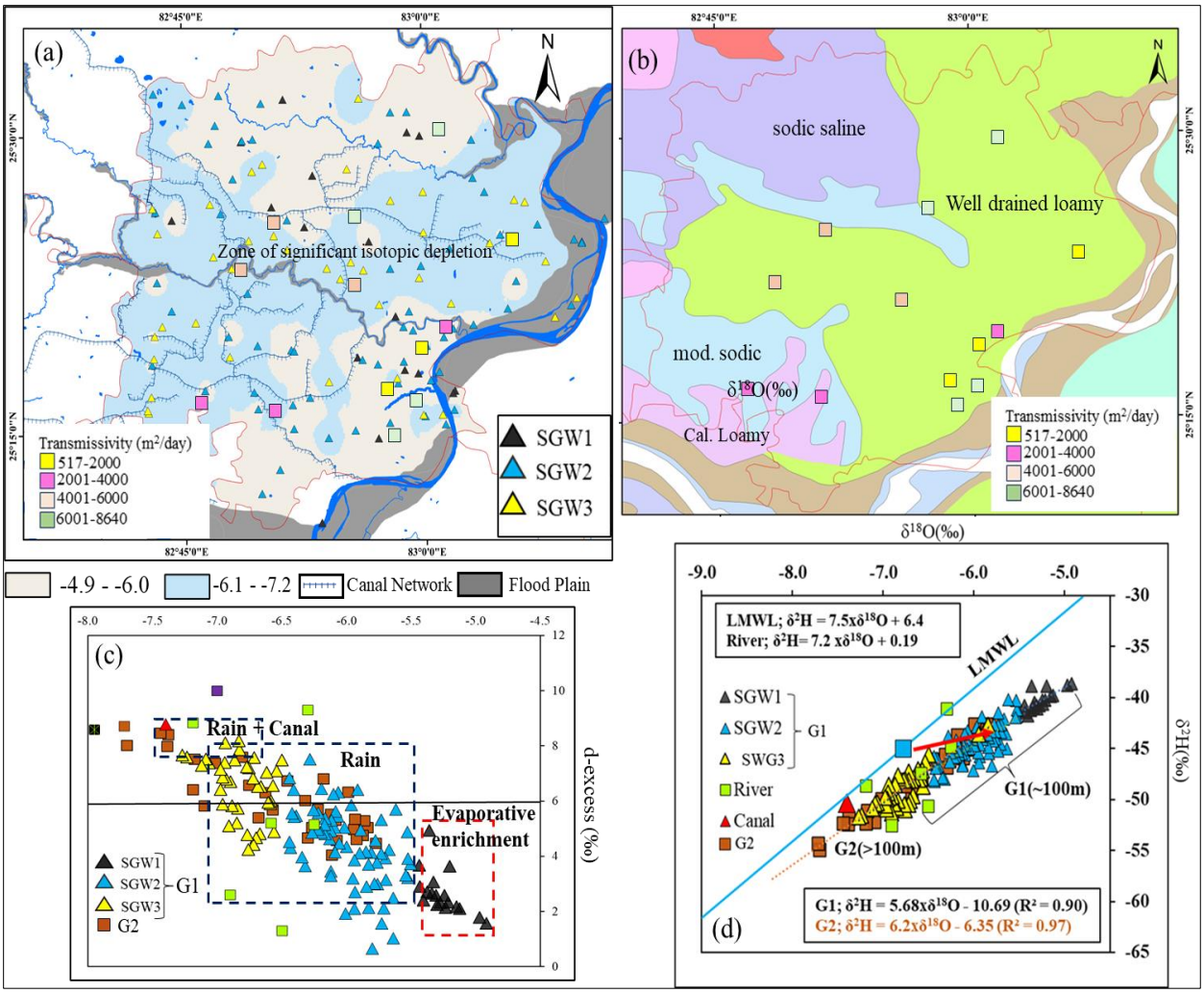


**Figure 4.20**: (a) $\delta^{18}O$ (‰) Isotopic variation of shallow groundwater in study area (interpolation), along with the sampling sites for G1(<100m) (further divided into SGW1, SGW2 & SGW3 (b) different soil layers along with the transmissivity values, (c) $\delta^{18}O$ vs. d-excess distinguishing the probable recharge mechanism of groundwater, and (d) cross plot $\delta^{18}O$ vs. $\delta^{2}H$ plot of group G1(3-100m) and G2 (>100-210m), with local meteoric water line, and surface water samples.

**Recharge zones and sources: (refer to figure 4.20)**

- The groundwater samples from the southeastern region (Urban Varanasi) fall under the SGW1 and SGW2 groups, characterized by an enriched isotopic composition. This region is densely populated and has a significant proportion of built-up areas. Hydrogeologically, the top of the aquifer in this area is overlain by a thick clay layer, which hinders infiltration and promotes surface runoff. As a result, water accumulates in nearby depressions, forming numerous ponds that are characteristic of this region (Patel et al., 2024). These hydrogeological and

anthropogenic conditions significantly influence the isotopic signatures of groundwater in this urban setting.

- Most groundwater samples from SGW3 observed in the central portion are comparatively depleted in isotopic signatures and high d excess values. The existing hydrogeological conditions in the southeastern region (Urban Varanasi) suggest three possible mechanisms for groundwater recharge:

    1. **Faster Recharge through Drained Soil**: The presence of drained soil layers facilitates quicker percolation of water into the subsurface, contributing to rapid groundwater recharge in certain pockets.

    2. **Recharge through Paleochannel**: The presence of paleochannels promotes lateral groundwater flow from distant locations, acting as a conduit for recharge from upstream areas.

    3. **Canal-Induced Recharge**: Seepage from nearby canals, combined with irrigation return flow, serves as an additional source of groundwater recharge, particularly in areas under agricultural influence.

- Most groundwater samples from SGW2 and SGW1 are spread in the north-western portion. The $\delta^{18}O$ and $\delta^{2}H$ signatures are comparatively enriched. The presence of thick clay content in the upper horizon, due to its impervious nature, significantly impedes infiltration, causing slow percolation of water into the groundwater system. Additionally, the low permeability of the clay layer leads to higher evaporation rates during the recharge process, further affecting the groundwater composition by enriching isotopic signatures and promoting evaporative conditions. This contributes to the observed hydrogeochemical characteristics in the region.

### 4.5.7 Use of $^{3}H$ dating to decipher groundwater age

The two groundwater wells located in the northwestern part of the study area, within the administrative boundary of the District Jaunpur, have tritium values of 2.83 (±0.17) TU and 3.22

(±0.17) TU, respectively (Figure 4.21a). Groundwater samples from the northwestern and central parts of the study area show tritium values ranging from 1.04 (±0.15) TU to 1.86 (±0.16) TU. In contrast, groundwater wells from Urban Varanasi exhibit tritium values between 0.05 (±0.15) TU and 0.78 (±0.15) TU.

This trend indicates that tritium values significantly decrease as groundwater moves from the northwestern part towards Varanasi city along the groundwater flow direction (Figure 4.21c–d). Furthermore, most of the deeper groundwater samples in the study area are a mixture of sub-modern to older water based on their tritium values (Figure 4.21c).

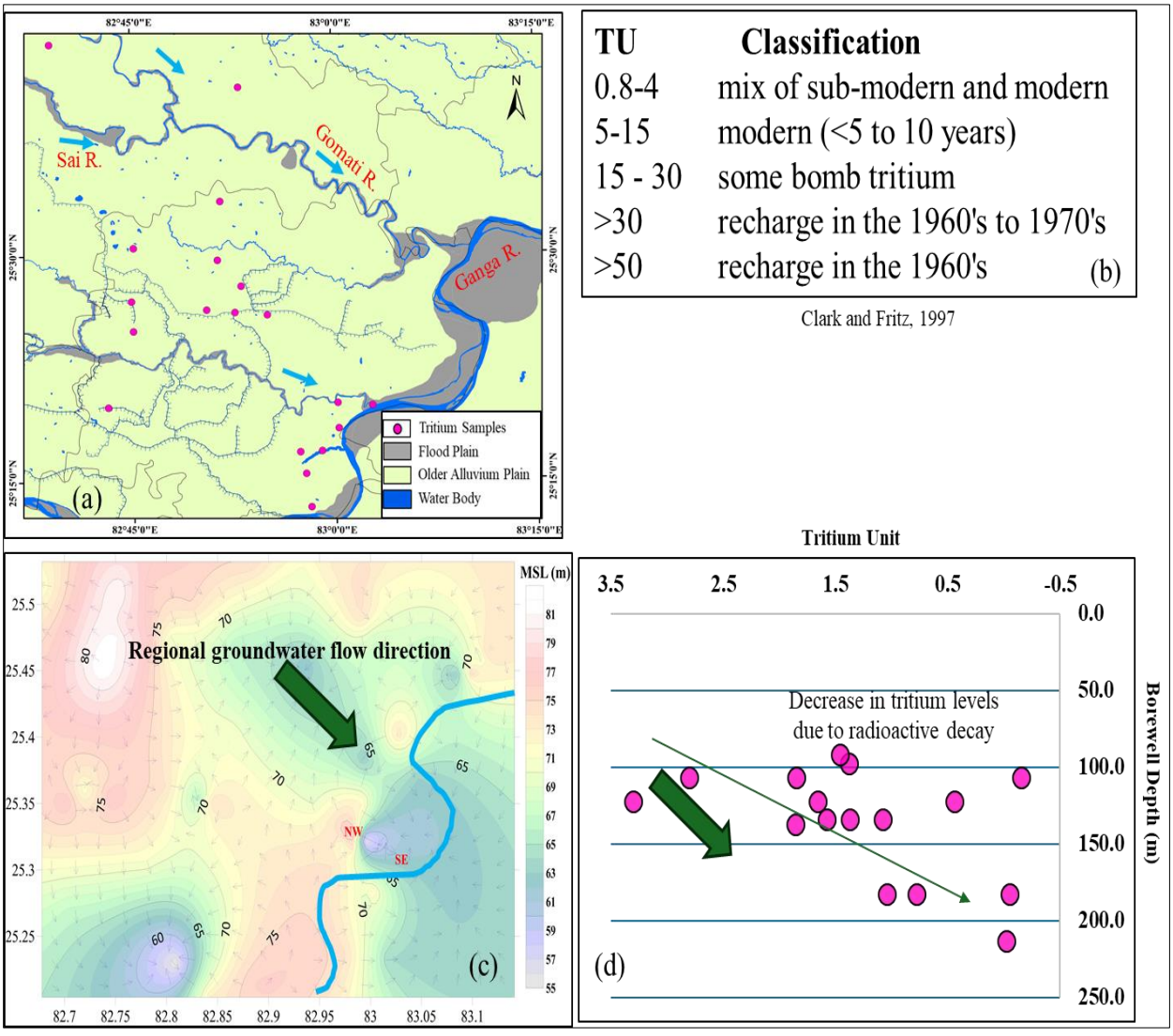


**Figure 4.21**: Groundwater samples for $^{3}H$ dating and groundwater flow direction showing decrease in the TU value along the regional flow direction

# 5. Major Conclusions

The following major conclusions are drawn from this study

- The hydrochemical data shows both spatial and vertical variability in groundwater hydrochemical parameters and quality. Comparing the major ions with the standards set by WHO (2017) and BIS (2012), it was found that 8% of the groundwater samples exceeded the permissible limit for fluoride ($F^-$), 5% for nitrate ($NO_3^-$), 2% for sulfate ($SO_4^{2-}$), and 12% for sodium ($Na^+$) ions.

- Approximately 98% of the groundwater samples were classified as hard to very hard, primarily due to the abundance of calcium ($Ca^{2+}$) and magnesium ($Mg^{2+}$) salts in the soil.

- The north-western portion of the study area is characterized by elevated concentrations of fluoride ($F^-$), bicarbonate ($HCO_3^-$), sodium ($Na^+$), and sulfate ($SO_4^{2-}$), while calcium ($Ca^{2+}$) and magnesium ($Mg^{2+}$) are ubiquitous in the groundwater. High concentrations of nitrate ($NO_3^-$) are predominantly associated with agricultural fields (75%) and human settlements (25%).

- Vertical variability is observed in the concentrations of nitrate, sulfate, chloride, which are often associated with high electrical conductivity (EC, µS/cm). High concentrations of these ions are found in groundwater samples up to a depth of 100 meters below ground level (mbgl). However, below 100 m and up to the maximum sampling depth of 210 m, the groundwater samples remain within the permissible limits, exhibiting minimal variation.

- The vertical variation of major ions in groundwater was further analyzed using the Mann-Whitney U-test, which helped classify the groundwater samples into two groups: Group G1 (<100 mbgl), representing the shallow to moderate depth of the first aquifer and Group G2 (>100-210 m), which taps the deeper part of the first aquifer and, in some cases, the second aquifer.

- The solute acquisition processes, inferred through molar ratios and forward mineral saturation indices, in conjunction with the soil/aquifer mineralogy, suggest that both silicates and secondary carbonates (calcite and dolomite) control the groundwater chemistry of both groups (G1 and G2).

- The presence of thick clay horizons, which act as ion exchange sites at shallow depths, increases the concentration of ions like $Na^+$ and $Ca^{2+}$ through ion exchange reactions. This effect is more prominent in group G1 (shallow groundwater), but limited in group G2 (deeper groundwater), likely due to the dominance of sand at greater depths.

- Chemometric, statistical and isotopic analyses suggest that fluoride ($F^-$) is primarily confined to shallow groundwater under alkaline water chemistry conditions. The release of $F^-$ is associated with high concentrations of $Na^+$ and $HCO_3^-$ ions and low concentrations of $Ca^{2+}$. This release is likely facilitated by the dissolution of minerals like fluorite, mica and amphiboles, which are abundant in the soil.

- The Groundwater Line (GWL) has a lower slope of 5.70 compared to the Indian Meteoric Water Line (IMWL, 7.93) and the Local Meteoric Water Line (LMWL, 7.5), indicating substantial evaporative enrichment in groundwater. This suggests that evaporation plays a significant role in the isotopic composition of shallow groundwater.

- Similar to hydrochemical attributes, the vertical profile of stable isotopic signatures of groundwater shows a wide variation up to the depth of 100 m, corresponding to group G1. The wide variation in isotopic values up to this depth indicates multiple recharge sources. Below 100 m, the δ18O and δ2H values of groundwater samples attenuate towards the average value of precipitation, which suggests that the primary recharge source at deeper depths is precipitation. The attenuation of isotopic values below 100 m depth indicates a more consistent and less variable recharge mechanism from precipitation.

- **Recharge zones and sources of recharge:**

  (i) **Northern Zone**: Groundwater in the northern zone belongs to the SGW2 and SGW1 categories, indicating higher evaporative enrichment due to slow groundwater recharge and shallow water table conditions.

  (ii) **Central Zone**: Groundwater samples in the central zone are characterized by comparatively depleted isotopic signatures (SGW3, SGW2 subgroups). The soil in this region is well-drained and loamy, with higher transmissivity, promoting faster recharge.

(iii) **Southeastern Region**: The southeastern region, influenced by urban activities, shows comparatively enriched isotopic signatures, falling under the SGW1 and SGW2 categories. This suggests that urbanization and land use changes have impacted the recharge process, likely causing more evaporative enrichment. Notably, the groundwater near the Ganga River, particularly along the Ghats, displays depleted $\delta^{18}O$ signatures, indicating limited groundwater-surface water interaction during peak monsoon. This suggests that during this period, groundwater and surface water interactions occur mainly in the hyporheic zone, indicating a limited extent of vertical exchange.

- **Groundwater age:** The lower tritium values, ranging from 0.05 (±0.15) TU to 0.78 (±0.15) TU, observed in groundwater samples from Varanasi city and near the banks of the Ganga River, suggest that the groundwater in these areas is older. These lower tritium values are consistent with the findings from stable isotope and water chemistry analyses, which indicate that the groundwater in these regions has a longer residence time, likely older than 50 years, especially in the deeper tubewell. The overall tritium data supports the idea that much of the deeper groundwater in the study area has a moderate to older age, which is important for understanding its sustainability and potential for over-extraction. Given the age of the groundwater, it is essential to focus on the deep groundwater dynamics to ensure its sustainable management. Furthermore, the findings indicate that the river recharge to groundwater is likely limited to the hyporheic zone, which is a shallow region where groundwater and surface water mix. This recharge mainly occurs during the peak monsoon season, highlighting the seasonal and limited interaction between the river and the groundwater system, particularly in the deeper aquifers. This underscores the need for careful management of groundwater, especially during periods of high demand or low recharge.

## 5.1 Recommendations

The **northwestern part** of the study area is characterized by **shallow groundwater** and **sodic saline soils** with elevated fluoride content. To address this issue, the affected areas can be treated with **gypsum mineral** ($CaSO_4 \cdot 2H_2O$), which helps in improving the soil structure. Additionally, **scraping, flushing, and leaching** are recommended as effective reclamation processes to reduce the sodicity and improve soil and water quality in the saline-affected regions.

**Nitrate ($NO_3^-$)** is **randomly distributed** across the study area, with a higher concentration in **tube wells**, particularly those using **Indian Mark handpumps**. To prevent further contamination of deeper groundwater horizons, it is crucial to implement **proper sealing** of the handpumps. This will help to avoid **nitrate leaching** from the surface and shallow groundwater to the deeper aquifers, ensuring better water quality and reducing the risk of nitrate-related health issues.

**References**


1. Akpataku, K. V., Gnazou, M. D., Djanéyé-Boundjou, G., Bawa, L. M., & Faye, S. (2020). Role of natural and anthropogenic influence on the salinization of groundwater from basement aquifers in the middle part of mono River Basin, Togo. Journal of Environmental Protection, 11(12), 1030-1051.

2. American Public Health Association, 2005. Standard Methods for the Examination of

3. Ansari, M. A., Noble, J., Deodhar, A., Kumar, U. S., 2022. Isotope hydrogeochemical models for assessing the hydrological processes in a part of the largest continental flood basalts province of India. Geoscience Frontiers, 132, 101336

4. BIS 2012. Indian standard drinking water specification, second revision ISO: 10500:2012. Bureau of Indian Standards. Drinking Water Sectional Committee, FAD25, New Delhi.

5. Bonsor, H. C., MacDonald, A. M., Ahmed, K. M., Burgess, W. G., Basharat, M., Calow, R. C., Zahid, A., 2017. Hydrogeological typologies of the Indo-Gangetic basin alluvial aquifer, South Asia. Hydrogeology Journal, 255, 1377-1406.

6. Census of India 2011 India. https://censusindia.gov.in/census.website/. Accessed 1 Feb 2023

7. Central Ground Water Board of India, 2010. Groundwater Year Book 2009-10.

8. Central Ground Water Board. (2020). Groundwater yearbook. Ministry of Water Resources, Government of India.

9. CGWB, 2017. Aquifer Mapping and Management of Ground Water Resources, Varanasi District, Uttar Pradesh. Central Ground Water Board, Ministry of Water Resources Government of India, Lucknow.

10. Chatterjee, J., Singh, S. K., 2022. Impact of Dissolution of Saline-Alkaline Soils on the Hydrochemistry and Erosion Rates of the Ganga River System. Geochemistry, Geophysics, Geosystems, 232, e2021GC009914.

11. Chidambaram, S., Karmegam, U., Prasanna, M. V., Sasidhar, P., & Vasanthavigar, M. (2011). A study on hydrochemical elucidation of coastal groundwater in and around Kalpakkam region, Southern India. Environmental Earth Sciences, 64, 1419-1431.

12. Craig, H., 1961. Isotopic variations in meteoric waters. Science, 133(3465), pp.1702-1703.

13. Dansgaard, W. (1964). Stable isotopes in precipitation. tellus, 16(4), 436-468.

14. Das, P., Mukherjee, A., Hussain, S. A., Jamal, M. S., Das, K., Shaw, A., Sengupta, P., 2021. Stable isotope dynamics of groundwater interactions with Ganges River. Hydrological Processes, 351, e14002.

15. Datta, P. S., Tyagi, S. K., & Chandrasekharan, H. (1991). Factors controlling stable isotope composition of rainfall in New Delhi, India. Journal of Hydrology, 128(1-4), 223-236.

16. Dey, S., Bhatt, D., Haq, S., & Mall, R. K. (2020). Potential impact of rainfall variability on groundwater resources: a case study in Uttar Pradesh, India. Arabian Journal of Geosciences, 13, 1-11.

17. Fetter, C. W., 1988, Applied hydrogeology: Columbus, Ohio, Merrill Publishing Company, 592 p.

18. Geological Survey of India. (2021). Evaluation of urban geochemical environment for heavy and trace elements in water and soil, Varanasi District, U.P. (Mission-IV). Northern Region, Lucknow.

19. Gibbs RJ (1970) Mechanisms controlling worlds water chemistry. Sci170:1088

20. Hudak, P. F., 1999. Chloride and nitrate distributions in the Hickory aquifer, Central Texas, USA. Environ. Int. 254, 393-401.

21. Jain, S. K. (2011). Population rise and growing water scarcity in India–revised estimates and required initiatives. Current Science, 101(3), 271-276.

22. Kanagaraj, G., & Elango, L. (2019). Chromium and fluoride contamination in groundwater around leather tanning industries in southern India: Implications from stable isotopic ratio δ53Cr/δ52Cr, geochemical and geostatistical modelling. Chemosphere, 220, 943-953.

23. Kumar, B., Rai, S. P., Kumar, U. S., Verma, S. K., Garg, P., Kumar, S. V., ... & Pande, N. G. (2010). Isotopic characteristics of Indian precipitation. Water Resources Research, 46(12).

24. Kumar, S., Joshi, S. K., Pant, N., Singh, S., Chakravorty, B., Saini, R. K., & Singh, V. (2021a). Hydrogeochemical evolution and groundwater recharge processes in arsenic enriched area in central Gangetic plain, India. Applied Geochemistry, 131, 105044.

25. Lapworth, D. J., Das, P., Shaw, A., Mukherjee, A., Civil, W., Petersen, J. O., MacDonald, A. M., 2018. Deep urban groundwater vulnerability in India revealed through the use of emerging organic contaminants and residence time tracers. Environmental Pollution, 240, 938-949.

26. Masoud, A. A., El-Horiny, M. M., Atwia, M. G., Gemail, K. S., Koike, K., 2018. Assessment of groundwater and soil quality degradation using multivariate and geostatistical analyses, Dakhla Oasis, Egypt. Journal of African Earth Sciences, 142, 64-81.

27. Mukherjee, A., & Fryar, A. E. (2008). Deeper groundwater chemistry and geochemical modeling of the arsenic affected western Bengal basin, West Bengal, India. Applied Geochemistry, 23(4), 863-894.

28. Mukherjee, A., Coomar, P., Sarkar, S., Johannesson, K. H., Fryar, A. E., Schreiber, M. E., ... & Vengosh, A. (2024). Arsenic and other geogenic contaminants in global groundwater. Nature Reviews Earth & Environment, 5(4), 312-328.

29. Mukherjee, A., Scanlon, B. R., Fryar, A. E., Saha, D., Ghosh, A., Chowdhuri, S., & Mishra, R. (2012). Solute chemistry and arsenic fate in aquifers between the Himalayan foothills and Indian craton (including central Gangetic plain): influence of geology and geomorphology. Geochimica et Cosmochimica Acta, 90, 283-302.

30. Nas, B., & Berktay, A. (2006). Groundwater contamination by nitrates in the city of Konya (Turkey): A GIS perspective. Journal of Environmental management, 79(1), 30-37.

31. Nizam, S., Virk, H. S., Sen, I. S., 2022. High levels of fluoride in groundwater from Northern parts of Indo-Gangetic plains reveals detrimental fluorosis health risks. Environ. Adv. 8, 100200.

32. Pant, N., Rai, S. P., Singh, R., Kumar, S., Saini, R. K., Purushothaman, P., ... & Pratap, K. (2021). Impact of geology and anthropogenic activities over the water quality with emphasis on fluoride in water scarce Lalitpur district of Bundelkhand region, India. Chemosphere, 279, 130496.

33. Patel, A., Rai, S. P., Puthiyottil, N., Singh, A. K., Noble, J., Singh, R., ... & Akpataku, K. V. (2024). Refining aquifer heterogeneity and understanding groundwater recharge sources in an intensively exploited agrarian dominated region of the Ganga Plain. Geoscience Frontiers, 15(4), 101808.

34. Rai, S. P., Akpataku, K. V., Noble, J., Patel, A., & Joshi, S. K. (2023). Hydrochemical evolution of groundwater in northwestern part of the Indo-Gangetic Basin, India: A geochemical and isotopic approach. Geoscience Frontiers, 14(6), 101676.

35. Rai, S. P., Noble, J., Singh, D., Rawat, Y. S., & Kumar, B. (2021). Spatiotemporal variability in stable isotopes of the Ganga River and factors affecting their distributions. Catena, 204, 105360.

36. Raju, N. J., Dey, S., & Das, K. (2009). Fluoride contamination in groundwaters of Sonbhadra district, Uttar Pradesh, India. Current science, 979-985.

37. Raju, N.J. (2012) Evaluation of Hydrogeochemical Processes in the Pleistocene Aquifers of Middle Ganga Plain, Uttar Pradesh, India. Environmental Earth Sciences, 65, 1291-1308.

38. Rivett, M. O., Buss, S. R., Morgan, P., Smith, J. W., & Bemment, C. D. (2008). Nitrate attenuation in groundwater: a review of biogeochemical controlling processes. Water research, 42(16), 4215-4232.

39. Rodell, M., Velicogna, I., & Famiglietti, J. S. (2009). Satellite-based estimates of groundwater depletion in India. Nature, 460(7258), 999-1002.

40. Rozanski, K., Araguás-Araguás, L., & Gonfiantini, R. (1993). Isotopic patterns in modern global precipitation. Climate change in continental isotopic records, 78, 1-36.

41. Samal, A. K., Mishra, P. K., Biswas, A., 2020. Assessment of origin and distribution of fluoride contamination in groundwater using an isotopic signature from a part of the Indo-Gangetic Plain (IGP), India. Hydro Res. 3, 75-84.

42. Senthilkumar, M., & Elango, L. (2013). Geochemical processes controlling the groundwater quality in lower Palar river basin, southern India. Journal of earth system science, 122, 419-432.

43. Shukla, U. K., Janardhana Raju, N., 2008. Migration of the Ganga River and its implication on hydro-geological potential of Varanasi area, UP, India. Journal of Earth System Science, 1174, 489-498

44. Shukla, U. K., Srivastava, P., Singh, I. B., 2012. Migration of the Ganga River and development of cliffs in the Varanasi region, India during the late Quaternary: Role of active tectonics. Geomorphology, 171, 101-113.

45. Singh, I. B., 1996. Geological evolution of Ganga Plain—an overview. Journal of the Palaeontological Society of India, 41, 99-137.

46. Singh, P., Saxena, A., 2022. Release of Fluoride in Groundwater from Various Rock Forming Minerals and Sandy Aquifer of Central Ganga Basin, India. Journal of the Geological Society of India, 981, 133-138

47. Singh, R. K., Sengupta, B., Bali, R., Shukla, B. P., Gurunadharao, V. V. S., & Srivatstava, R. (2009). Identification and mapping of chromium (VI) plume in groundwater for remediation: A case study at Kanpur, Uttar Pradesh. Journal of the Geological Society of India, 74, 49-57.

48. Stallard, R. F., & Edmond, J. M. (1987). Geochemistry of the Amazon: 3. Weathering chemistry and limits to dissolved inputs. Journal of Geophysical Research: Oceans, 92(C8), 8293-8302.

49. Tiwari, V. M., Wahr, J., & Swenson, S. (2009). Dwindling groundwater resources in northern India, from satellite gravity observations. Geophysical Research Letters, 36(18).

50. UNICEF (2013). "Water in India: Situation and prospects." UNICEF, New Delhi.

51. WHO, 2017. Guidelines for drinking-water quality, 4th edition. World Health Organization, Geneva.

52. World Health Organization, 2011. Guidelines for Drinking-Water Quality, 4th Ed., World Health Organization, Geneva.

53. Zhou, Z., Ansems, N., & Torfs, P. (2015). A global assessment of nitrate contamination in groundwater. International Groundwater Resources Assessment Center. Internship report, 4.